EMPIR

EURAMET

The EMPIR initiative is co-funded by the European Union's Horizon 2020 research and innovation programme and the EMPIR Participating States

18SIP02 5GRFEX D2

Good Practice Guide (GPG) for traceable RF-EMF measurement and data processing methods/protocols of 5G Massive MIMO base station systems

Project Number: JRP 18SIP02

Project Title: Metrology for RF exposure from Massive MIMO 5G base station: Impact on 5G network deployment (5GRFEX)

Document Type: Good Practice Guide

Authors: Tian Hong Loh, Yunsong Gui, David Cheadle, Fabien Heliot, Sung-won Moon, and Michael Dieudonne

Lead Partner: NPL

Participating Partners: SURREY, Keysight DK

Due Date: October 2021

Submitted Date: December 2021

NPL National Physical Laboratory

UNIVERSITY OF SURREY

KEYSIGHT TECHNOLOGIES

Table of Contents

List of Abbreviations

3GPP	3rd Generation Partnership Project
2G	2nd Generation Wireless Systems
3G	3rd Generation Wireless Systems
4G	4th Generation Wireless Systems
5G	5th Generation Wireless Systems
CIR	Channel Impulse Response
CP-OFDM	Cyclic Prefix – Orthogonal Frequency Division Multiplexingmodulation
CW	Continuous Wave
EMF	Electromagnetic Field
ERP	Effective Radiated Power
FDM	Frequency-Division Multiplexing
FR1	Frequency Range 1
FR2	Frequency Range 2
GSMA	Groupe Spéciale Mobile Association
ICNIRP	International Commission on Non-Ionizing Radiation Protection
IEC	International Electrotechnical Commission
IEEE	Institute of Electrical and Electronics Engineers
ITU	International Telecommunication Union
MIMO	Multiple-Input-Multiple-Output transmission
ML	Maximum Likelihood
mMIMO	Massive Multiple-Input-Multiple-Output
NR	New Radio
OFDM	Orthogonal Frequency-Division Multiplexing
OTA	Over-The-Air
PRB	Physical Resource Block
RE	Resource Element
RF	Radio Frequency
Rx	Receiving end
SA	Spectrum Analyser
SSB	Synchronisation Signal Block
SSS	Secondary Synchronization Signal

Tx	Transmitting end
UE	User Equipment
VNA	Vector Network Analyser
VSG	Vector Signal Generator

1 Scope of the document

This document, namely, Deliverable 1 (D2), serves as a good practica guide (GPG) on work carried out under work package 2 (WP2) of the European Association of National Measurement Institutes (EURAMET) funded support for impact (SIP) project – 18SIP02, entitled “Metrology for RF exposure from Massive MIMO 5G base station: Impact on 5G network deployment (5GRFEX)”. This GPG presents the guides for traceable radio frequency electromagnetic field (RF-EMF) measurement and data processing methods/protocols of massive multiple-input-multiple-output (mMIMO) systems for fifth generation (5G) base station applications. Also, the details of the relevant calibration procedures and setup for mMIMO beamforming and RF-EMF measurement systems are provided. The discussion on the hints and tips while carrying out the empirical measurements under A1.2.2 (indoor and outdoor / fixed beamforming) and A2.1.1 (outdoor / adaptive beamforming) (as shown in the Deliverable Report D1) will also be included.

2 Introduction

2.1 Background

Massive multiple-input–multiple-output (MIMO) antenna systems are one of the key enablers for the fifth generation (5G) of cellular systems and are so far one of the main differences between 5G and the previous generations at the physical layer. The idea behind massive MIMO (mMIMO) is to equip base stations (BSs) with a very large number of antenna elements to create narrow directional beams for transmitting information to different users on the same frequency/time resource and, hence, greatly improve the spectral efficiency of the system. New technology comes with new challenges, the high directionality of the transmission when using mMIMO and the complex dynamic operation of new radio (NR) resource grid, compares to existing cellular technologies, raises questions about the level of radio frequency (RF)-exposure such system generates on the general population and how to evaluate this exposure. Indeed, traditional BS technology radiates RF power more or less uniformly in all directions, while BSs relying on mMIMO focus their power on the user equipment (UE) devices, such that the distribution of power, which becomes scenario related (e.g. position of the UE, duration of usage), is not necessarily uniform anymore. Hence, it is expected that the RF-exposure would be quite different when mMIMO technology is used at the BS instead of the traditional sectorised BS. In turn, it creates a need for the current exposure regulation, which lacks of harmonisation and is highly conservative in some parts of the world, to be updated in order to fully reflect the way mMIMO operates and generates RF-exposure on the general population.

2.2 Motivation for 5G RF-exposure new metrology and guidelines

The new generation of mobile networks, which promises among other things higher data rate, lower latency and higher reliability than the previous generation, is being rolled out (in 2020) throughout the world. The roll-out is driven by the demand for higher speed communication for a range of diverse applications for the general public and industries. As it is the casewith previousmobile technology, 5G uses non-ionising RF to operate, and the public concerns over the potential health risks from RFexposure generated by mobile network equipment, such as BSs, have led in the past to very strict RF-exposure compliance regulation in some parts of the world. In addition, the level of RF-exposure experienced by the general public is foreseen to steadily increase in the decades to come [1], while the impact of non-ionised electromagnetic field (EMF) radiations on the human body is still a debated issue in the scientific community [2], such that concerns about RF-exposure in the general public are currently being reignited by the roll-out of the 5Gtechnology, despite the strict regulation.

At the international level, the International Commission on Non-Ionizing Radiation Protection (ICNIRP) [3] provides guidelines on RF-exposure for both mobile network equipment, e.g. BS, and mobile network devices, e.g. UE. These guidelines have been used to form regulations in many countries and regions in the world (including Europe), however, in an un-harmonised and often stringent manner to deal with the concerns of the population in countries, regions and even cities. For instance, in Europe, at the country level, Switzerland and Italy have different RF-exposure limits at 4 and 6 V/m, respectively, while similarly at the city level, Paris and Brussels have different RF-exposure indoor limits, i.e. 5 and 6 V/m, respectively. All these limits go well beyond the guidelines of 61 V/m set by ICNIRP for the general public [3]. This un-harmonised and stringent regulatory framework obviously creates challenges for the deployment of new BS technology like mMIMO in 5G. It is expected to affect the design and deployment of effective 5G networks [4, 5] – meaning that 5G communication systems may not work in some geographical areas and that the seamless connectivity promised by 5G turns out to be impossible to implement. It is also likely to impact the coverage and quality of service provided to the consumers as it has already been the case to some extent in the fourth generation (4G) of mobile networks [4, 6].

The traditional approach utilised by operators for meeting the RF-exposure regulations in the third-generation (3G) and the 4G of mobile networks, in a particular geographical area, is to rely on the concept of exclusion zone, also known as compliance boundary [7]. An exclusion zone is an area around a BS where the general public is not allowed access to. It is traditionally defined, in a conservative way, based on the theoretical maximum power that can be transmitted in all possible directions for a defined time-period of usually several minutes [8]. In effect, it assumes uniform power/energy distribution around the BS. This might be a correct assumption for sectorised 4G BS, but not anymore for 5G BS due to the usage of the mMIMO technology, such that the current way of defining an exclusion zone is deemed to not be fit for purpose anymore [9]. Indeed, the way mMIMO BSs operate is quite different from previous generations of BSs; 3G or 4G BSs were designed to radiate power in an omnidirectional (over 360°) or in sectorised manner (over typically 120°), respectively, to ensure a more or less uniform coverage of their transmit signals within a geographical area, while mMIMO BSs are designed to transmit signals in a very directive manner (e.g. by using 5° narrow beam) with higher antenna gain, i.e. by relying on beamforming. Hence, applying the current approach, i.e. by considering the theoretical maximum transmit power in all the directions, for defining the exclusion zone of mMIMO BS would result in unrealistic large exclusion zone areas, which would prevent operators from deploying 5G BSs at sites with pre-existing 3G and 4G BSs [10]. Another key difference with traditional BSs is that beamforming update and UE scheduling can be done in a matter of a few milliseconds, i.e. a BS can transmit a beam in one direction for a few milliseconds and then change the direction of this beam for the next few millisecond, such that computing the RF-exposure of a transmission based on an average over several minutes does not make that much sense anymore. Another important aspect to take into account is that an mMIMO BS might not be fully loaded every millisecond and when multiple users are served simultaneously on different beams (in different directions), the transmit power is split amongst these beams.

2.3 RF-EMF standards, regulations and Public -EMF reports

In the light of the obvious shortcomings of the current RF-exposure metrology and its implications on the ability of 5G mMIMO BS to meet the current regulations, which are directly linked to this metrology, there is a clear need to design and adopt a new metrology and update/reshape the regulations accordingly. In this regard, it is envisaged that a robust RF-exposure metrology for 5G mMIMO system should rely on suitable statistical approaches. For instance, approaches based on rigorous scientific evidences that ensure a good balance between user experience and public safety, such that user services requiring high-power beams are only utilised on a need-to-basis [4, 9]. A few years ago, the International Electrotechnical Commission (IEC), which is in charge of standardising the method for setting up BS exclusion zone, introduced a statistical approach to do so [8]. The

approach evaluates in a more accurate manner the actual transmit power that is radiated in realistic scenarios, such that this power is defined as the 95th percentile of the measured values instead of the theoretical maximum value. Interestingly, it turns out that the exclusion for mMIMO BS is smaller when using this statistical method contrary to the traditional method. Similar conclusions have then been reached in [9, 11], where the benefits of using a statistical approach for assessing the exclusion zone around the BS have been studied. The work in [9] proposed a statistical model of the time-averaged maximum power (i.e. defined as in [8]) when considering BS utilisation, mMIMO technology, time-division duplexing (TDD) and spatial distribution of the UEs. Their results show that the exclusion zone can be reduced by 15% as compared to the traditional method based on maximum transmit power. Meanwhile, the work in [11] has evaluated by means of system level simulations how the power is focused when an mMIMO BS is used and realistic assumptions regarding the UE distribution and traffic models are taken into account. Based on the cumulative distribution function of the mMIMO BS transmit power, the exclusion zone has been calculated and it turns out to be half the size of the one obtained by the traditional method.

Meanwhile, measurement campaigns of operating 5G BSs have been performed in countries where 5G is already deployed, e.g. the United Kingdom [12], France [13], Australia [14], to better understand the RF-exposure generated by mMIMO BSs in real environments. In [12], the RF-exposure level of 5G BSs in different test sites throughout the United Kingdom has been evaluated by using a field strength analyser attached to an isotropic field probe and following a procedure based on the in situ RF-exposure measurement method set out by IEC. It was found that the RF-exposure level from a typical 5G BS is only a small fraction of the ICNIRP guideline value, with the highest level recorded being approximately only 1.5% of this value. In [13], similar to [12], the RF-exposure level of 5G BSs in different test sites has been evaluated and a new wave exposure measurement indicator considering the specific characteristics of 5G networks has been proposed based on these evaluations. Accordingly, it is foreseen in [13] that the RF-exposure of a 5G BS should be at worst similar to that a current 4G BS and at best 35% lower to it. In [14], experimental data on the spatial distribution of 5G BS transmit power have been collected over a 24-h period. These data have revealed that assuming constant peak power transmission in a fixed beam-direction leads to an unrealistic EMF exposure assessment. They also indicate that the maximum time-averaged power per beam direction is well below the theoretical maximum, i.e. in-line with the prediction of the statistical model of [11], since they lead to an exclusion zone half the size of the one calculated by using the theoretical maximum power.

Despite the aforementioned works on defining measurement methods and exclusion zone for 5G BS, the definition of robust and effective model and/or experimental-based methods is still being an open problem under evaluation by international organisations. The IEC Technical Committee 106 and IEEE Technical Committee 34 have established IEEE/IEC joint working groups that develop standards in the area of EMF compliance assessment for 5G technology. In addition, the internal telecommunication union-T Study Group 5 is also closely collaborating with these technical committees. More works need to be done to fully understand how the RF-exposure generated by mMIMO BS fluctuates as a function of the environment, i.e. spatial and temporal variations (note that most measurement campaigns using real 5G BS are based on outdoor data), user traffic profile and number as well as positions of the users by using more traceable and reproducible methods in a control environment. An example of such method is detailed in the following, where a 5G mMIMO testbed, based on software-defined radio (SDR) and hence fully reconfigurable, has been set up and utilised to build an experimental-based statistical model of the RF-exposure of 5G BS [15, 16].

3 RF-EMF measurement techniques

The 5G mobile network introduces dramatic improvements with respect to the previous technologies. Features such as variable mMIMO, bandwidth parts, numerology, and TDD will extend the

capabilities of the 5G wireless systems to allow for an efficient and optimized use of transmission power and radio resource as well as influence the measurement techniques used to assess the compliance with general public RF-EMF exposure limits. Over the past few years, there have been a few publications discussing how to assess the RF-EMF exposure levels from 5G BS [9] – [11], [18] – [20]. These studies include numerical studies, and some preliminary measurements. On standardization, the IEC has published in IEC 62232 [8] the widely accepted RF-EMF measurement techniques that address the evaluation of RF field strength, power density and specific absorption rate (SAR) levels in the vicinity of radiocommunication BS radiating in the frequency range from 110 MHz to 100 GHz. Also, in IEC TR 62669 [21], several case studies have been provided in support of IEC 62232. Note that, in this GPG, the focus is given on the discussion of the RF-EMF measurement techniques for RF field strength.

The assessment principle in the published the IEC 62232 standard is to measurement the power received by a calibrated antenna from a "constant RF source", typically a pilot signal, and applying an extrapolation formula as describe in [8] Annex B.5. Such method ensures that the resulting field is the maximum obtainable at the location for the considered RF source. Nevetheless, the suitability of this kind of approach is still under investigation for 5G technology despite that it has been standardized for second-generation (2G), 3G, and 4G technologies as described in Appendix F – 'Technology-specific guidance' in [8]. Especially, an important problem affecting the RF-EMF measurement of 5G signals is the variation of power associated to antenna sweeping due to the sophisticated use of the space-time resources offered by the communication channel [22]. One notes that RF-EMF measurement of 4G signals takes advantage of the Reference Signal that has constant power, as reference for the extrapolation technique whereby the variable power of the synchronization signal blocks (SSBs) in the 5G signal present the application of the 4G procedure. For 5G NR transmission, the international standard body – 3GPP (Third-Generation Partnership Project) [23] has adopted CP-OFDM (Cyclic Prefix – Orthogonal Frequency Division Multiplexingmodulation) where OFDM is a frequency-division multiplexing (FDM) using many closely spaced orthogonal subcarriers with a proper guard interval to eliminate intersymbol interference.

The following shows the relevant RF-EMF measurement techniques for assessment of 5G BS operation based on the RF field strength and SSB evaluations. Both these evaluations are typically based on suitable statistical approaches with the use of a field strength analyser attached to an isotropic field probe.

3.1 Field strength method

Field strength probes are often being used to measure the E-field or magnetic field (H-field) strength. In practice, the characteristaion of field strength usually only require measurement of either E-field H-field. Typically, a field strength probe consists of three isotropic mutually orthogonal sensors, which together provide a vector sum of the field magnitude, independent of polarization or direction of propagation of the electromagnetic (EM) wave. Field strength probes are not designed to be calculable but their calibration require setting up a known EM field defined by parameters that can be readily made traceable to national standards. These parameters are in effect that of power, impedance, attenuation and length. The probe sensitivity (normally reported as a correction factor in terms of the measured and true 'known' field) along each axis can be measured separately by aligning each sensor in turn with the calibrating field inclined at an angle of 54.7° to its handle. i.e. every 120 degrees, one of the axes is positioned perpendicular in the generated field. Figure 2 and Figure 2 show, respectively, the illustrative setup diagram and the photo of a typical probe calibration setup in the NPL Power Flux Density (PFD) laboratory .

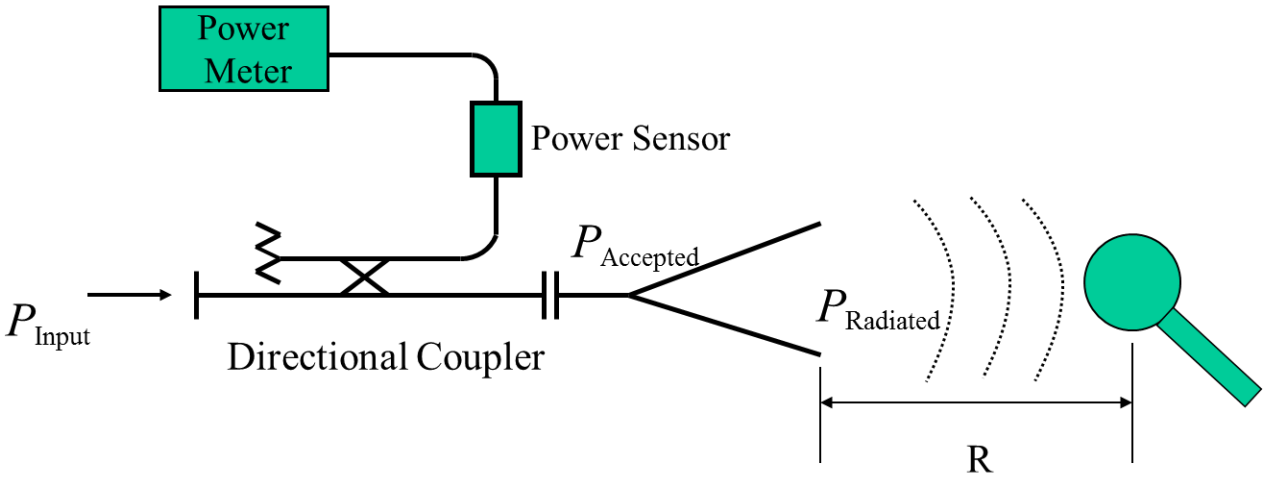

Figure 1 *Typical probe calibration setup in NPL PFD laboratory.*

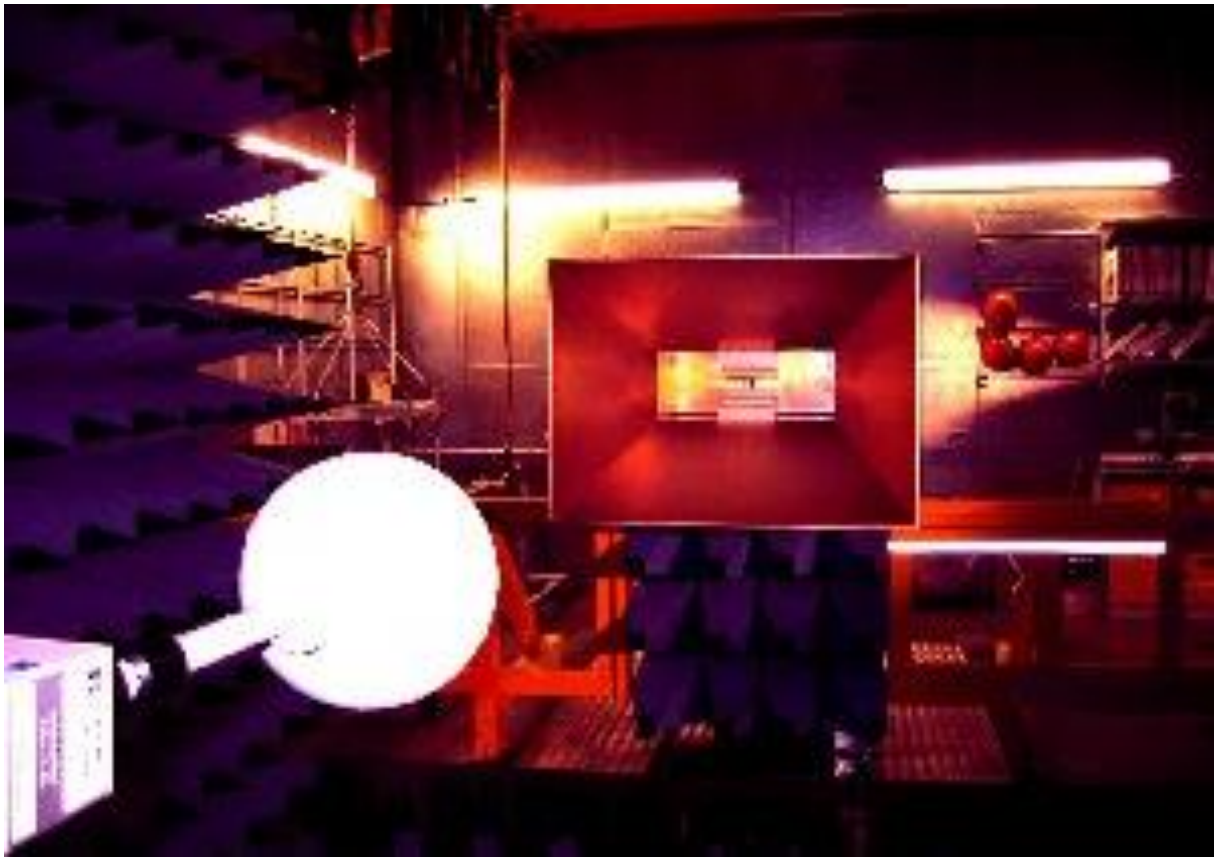

Figure 2 *Typical probe calibration setup in NPL PFD laboratory.*

As depicted in Figure 2, to produce a calculable plane-wave field, the output of a RF source is fed to a directional coupler. A calibrated power meter on the side arm of the coupler monitors the power incident on an antenna connected to the output of the coupler. Knowing the gain of the antenna at the distance at which the calibration is performed, it is then possible to evaluate the measured E-field strength using Equation (1) whereby the calibrated RF-EMF could be obtained using Equation 2.

$$E_{\text{Measured}} = \sqrt{\frac{P_{\text{Accepted}} \times G \times \eta_0}{4\pi R^2}} \quad (1)$$

where $\eta_0 = 377\ \Omega$ is the wave impedance of a plane wave in free space,

P_{Accepted} is the power accepted by the antenna from the coupler, and

G is the gain of the antenna at range R.

$$\begin{aligned} EMF &= \left|E_{\text{Total}_{\text{Calibrated}}}\right| = \sqrt{\left(E_{x_{\text{Calibrated}}}\right)^2 + \left(E_{y_{\text{Calibrated}}}\right)^2 + \left(E_{z_{\text{Calibrated}}}\right)^2} \\ &= \sqrt{\left(E_{x_{Measured}} \times CF_x\right)^2 + \left(E_{y_{Measured}} \times CF_y\right)^2 + \left(E_{z_{Measured}} \times CF_z\right)^2} \\ &= \sqrt{\left(\sqrt{\eta_0 CP_{x_{Measured}}} \times CF_x\right)^2 + \left(\sqrt{\eta_0 CP_{y_{Measured}}} \times CF_y\right)^2 + \left(\sqrt{\eta_0 CP_{z_{Measured}}} \times CF_z\right)^2} \\ &= \sqrt{\eta_0}\sqrt{CP_{x_{Measured}} \times {CF_x}^2 + CP_{y_{Measured}} \times {CF_y}^2 + CP_{z_{Measured}} \times {CF_x}^2} \end{aligned} \quad (2)$$

where $E_{i_{\text{Calibrated}}}$ for $i = x, y, z$, are the calibrated E-field in *x*-, *y*-, & *z*-axis respectively,

$E_{i_{\text{Measured}}}$ for $i = x, y, z$, are the measured E-field in *x*-, *y*-, & *z*-axis respectively,

$CP_{i_{\text{Measured}}}$ for $i = x, y, z$, are the measured channel power in *x*-, *y*-, & *z*-axis respectively,

CF_i for $i = x, y, z$, are the correction factor in *x*-, *y*-, & *z*-axis respectively.

3.2 Synchronization signal block (SSB) method

There has been concerns about the use of the maximum worst-case exposure to quantify the exposure of 5G BSs [11], [14]. Over the past few years, to address the 5G RF-EMF exposure measurement challenges, the principles based on the measurement of the synchronisation signal block (SSB) have been proposed in several contributions [8], [24] – [27]. In 5G, SSB consists of a block of 240 subcarriers and 4 OFDM symbols containing the Primary Synchronisation Signal (PSS), the Secondary Synchronisation Signal (SSS), the Physical broadcst channel (PBCH) and the PBCH demodulation reference signal (PBCH DM-RS) [22] (see Figure 3). The SSBs are grouped in block patterns called SS bursts (see illustration in Figure). Compared with the traditional field strength method which measures the gross receiving RF signal power in a specific frequency bandwidth and a specific time duration window no matter what sources of the RF signals are, SSB based method measures the RF signal power of impinging into the probe from the object BS by extracting object BS's SSS part from the receiving signal with the aid of the unique scrambling sequence for each BS and measuring its Reference Signals Received power (RSRP) and further calculating the relevant 5G BS RF-EMF level. The following shows two SSB based methodologies proposed by IEC and METAS (national metrology institute of Switzerland), respectively. These methodologies are slightly different in implementation approaches.

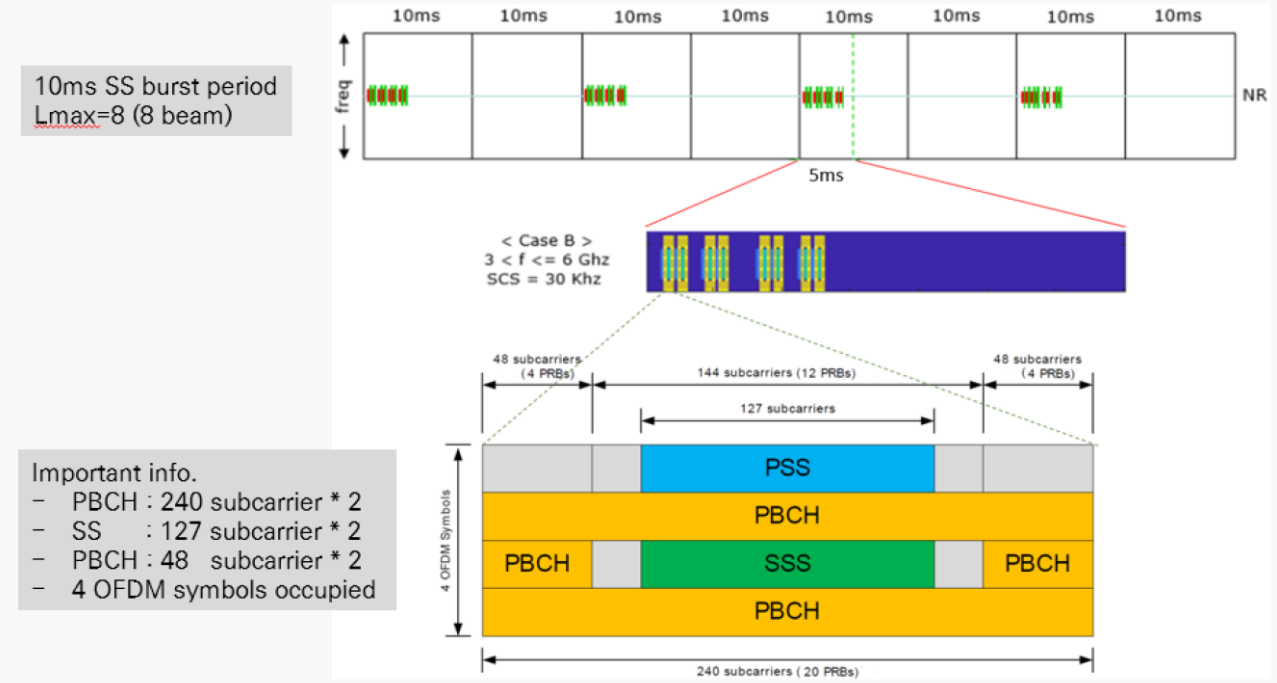

Figure 3 *Configuration of the SS burst slots and SS/PBCH blocks in the 5G NR signal.*

3.2.1 Methodology based on IEC

The SSB based method has recently being proposed by Korea's National Radio Research Agency (RRA) [27] – [28] and together with AGOS Ltd. an extrapolation technique for maximum field strength estimation for 5G NR FR1 has been proposed for adaptation in IEC 62232 [29], which extrapolate the RF-EMF level from measured RSRP per resource element (RE) of the SSB. The measurements require that the system bandwidth and center frequency of the target NR carrier is set. The extrapolated maximum electric field strength, E_{asmt}, is defined by Equation (3), which is envisaged applicable for evaluation of RF-EMF for mMIMO beamforming system.

$$\begin{aligned} E_{\mathrm{asmt}} &= E_{\mathrm{SSB}} \times \sqrt{F_{\mathrm{extSSB}}} \\ &= E_{\mathrm{SSB}} \times \sqrt{F_{\mathrm{BW}} \times F_{\mathrm{PR}} \times F_{\mathrm{TDC}}} \\ &= E_{\mathrm{SSB}} \times \sqrt{F_{\mathrm{ExtBeam}} \times F_{\mathrm{BW}} \times F_{\mathrm{PR}} \times F_{\mathrm{TDC}}} \end{aligned} \quad (3)$$

where

E_{SSB} is the field level (V/m) per RE of the SSB

F_{TDC} is the technology duty cycle

F_{PR} is the power reduction if the actual max. approach is used, otherwise it is set to 1

F_{BW} is the total number of subcarriers within the carrier bandwidth

F_{extSSB} is the extrapolation factor for the SSB

F_{ExtBeam} is the extrapolation factor corresponding to the ratio of the Effective Isotropic Radiated Power (EIRP) envelop of all traffic beams to the EIRP envelop of the broadcast signal at the direction to the measurement location

When the power allocated to any subcarrier is the same, F_{BW} corresponds to the number of subcarriers for the system bandwidth of the target BS. Equations (4) and (5) show, respectively, the detail mathetical definition of F_{BW} and F_{TDC}.

$$F_{\mathrm{BW}} = N_{\mathrm{SC}}^{\mathrm{RB}} \times N_{\mathrm{RB}}^{\mathrm{BW}} \tag{4}$$

$$F_{\mathrm{TDC}} = \frac{N_{\mathrm{Occupied}}^{\mathrm{RE}}}{N_{\mathrm{Total}}^{\mathrm{RE}}} \tag{5}$$

$$F_{\mathrm{PR}} = \frac{\mathrm{D}_{\mathrm{AMAX\ data\ rate}}}{\mathrm{D}_{\mathrm{TMAX\ data\ rate}}} \tag{6}$$

where

$N_{\mathrm{SC}}^{\mathrm{RB}}$	is the number of subcarriers in one resource block (RB)
$N_{\mathrm{RB}}^{\mathrm{BW}}$	is the maximum number of RBs in transmitted frequency bandwidth
$N_{\mathrm{Total}}^{\mathrm{RE}}$	is the total number of REs in one SS burst period
$N_{\mathrm{Occupied}}^{\mathrm{RE}}$	is the total number of occupied REs in one SS burst period
$\mathrm{D}_{\mathrm{AMAX\ data\ rate}}$	is the actual maximum average data rate the actual environment (Mbps)
$\mathrm{D}_{\mathrm{TMAX\ data\ rate}}$	is the theoretical maximum data rate (Mbps)

Note that Equations (5) and (6) are proposed by AGOS to IEC62232 as defined in Section B.9.2 and 6.2.3 of IEC62232:2021, respectively. As shown in Equation (6), the definition of the power reduction factor is calculated as the ratio of the theoretical maximum data throughput of the network to the actual available data throughput. It is considered to avoid the overestimation from the result of extrapolation. The detailed evaluation of $N_{\mathrm{Total}}^{\mathrm{RE}}$ and $N_{\mathrm{Occupied}}^{\mathrm{RE}}$ are shown in Equations (7) and (8), respectively.

$$N_{\mathrm{Total}}^{\mathrm{RE}} = N_{\mathrm{SC}}^{\mathrm{RB}} \times N_{\mathrm{RB}} \times N_{\mathrm{Symb}}^{\mathrm{Slot}} \times N_{\mathrm{Slot}} \tag{7}$$

$$N_{\mathrm{Occupled}}^{\mathrm{RE}} = N_{\mathrm{RE,down}}^{\mathrm{PDSCH}} - N_{\mathrm{RE,Empty}}^{\mathrm{SSB}} \tag{8}$$

where

N_{RB}	is the number of RB in the transmit bandwidth
$N_{\mathrm{Symb}}^{\mathrm{Slot}}$	is the number of symbols in one slot
N_{Slot}	is the toal number of slots in one SS burst period
$N_{\mathrm{RE,down}}^{\mathrm{PDSCH}}$	is the total number of RE in the down link of PDSCH
$N_{\mathrm{RE,Empty}}^{\mathrm{SSB}}$	is the total number of RE in the down link of slots including SSB within one SS burst period

Figure 4 and Figure 5 show, respectively, an illustrative example on how to calculate the power occupied REs numbers in one SS burst period and an overview of the procedure for evaluation of $\mathrm{E}_{\mathrm{asmt}}$.

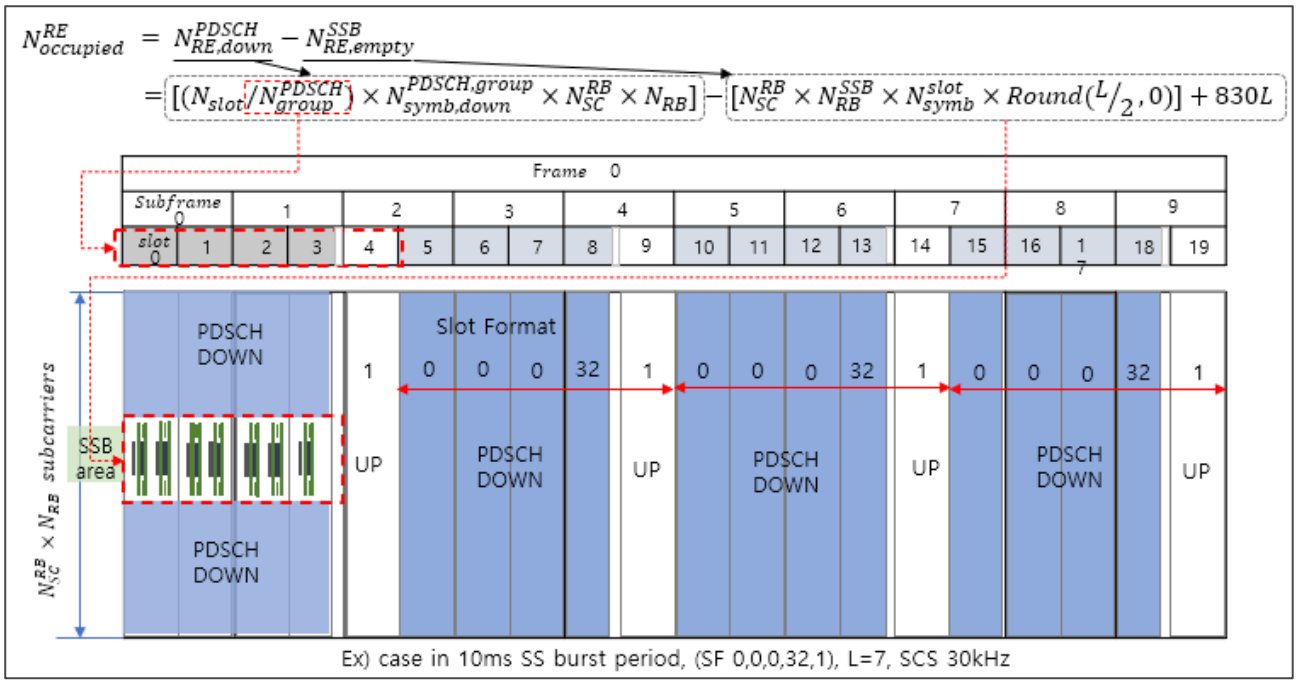

Figure 4 *Illustrative example for the calculation of power occupied REs numbers in one SS burst period.*

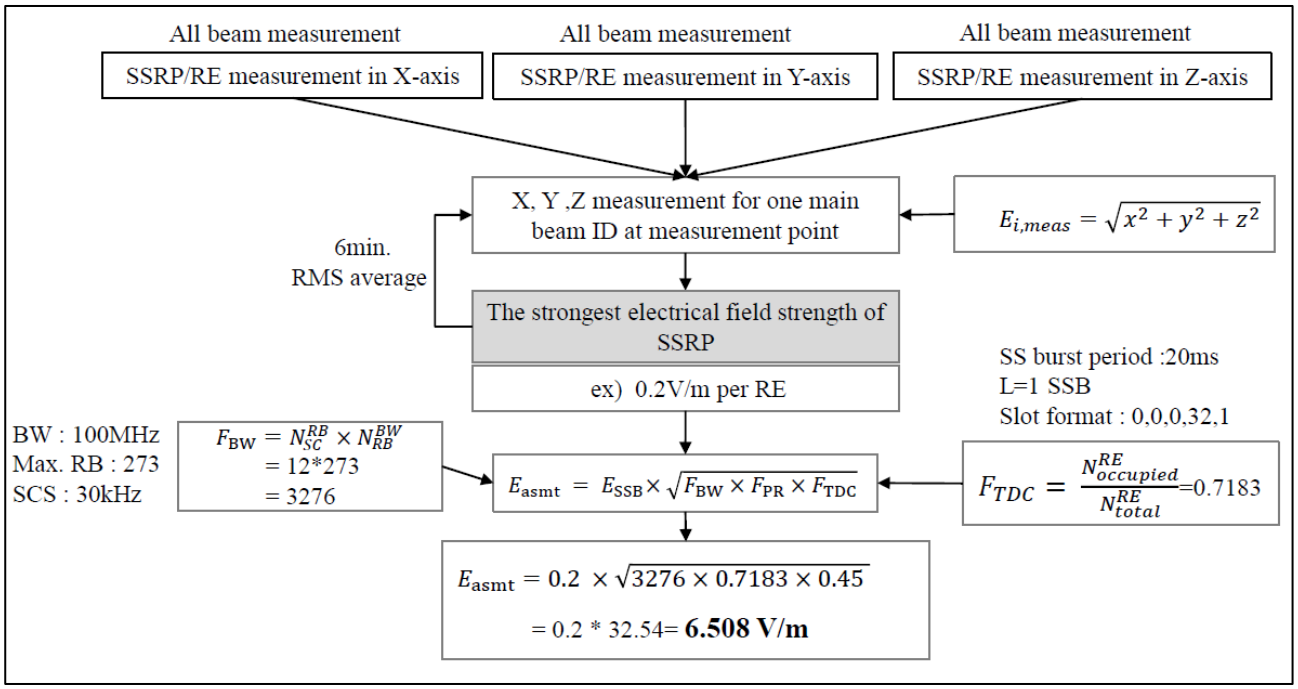

Figure 5 *Overview of the procedure for evaluation of* E_{asmt}.

The theoretical maximum data rate in 5G NR, D_{TMAX} (in Mbps), must have the equation including carrier aggregation, MIMO layers, bit per modulation symbol, scaling factor, maximum code rate, subcarrier configuration, frequency bandwidth, physical resource blocks (PRBs), overhead and slot allocation as in Section F7 of 3GPP 38.306 (see Equation (9)).

$$\mathrm{D_{TMAX}} = 10^{-6} \times \sum_{j=1}^{J} \left[v_{\mathrm{Layers}}^{(j)} \times Q_m^{(j)} \times f^{(j)} \times R_{\max} \times \frac{N_{\mathrm{PRB}}^{\mathrm{BW}(j),\mu} \times 12}{T_s^{\mu}} \times (1 - OH^{(j)}) \times SA_{\mathrm{DL}} \right] \quad (9)$$

Where

J	is the number of aggregated component carriers, maximum number (3GPP 38.802)
$v_{\mathrm{Layers}}^{(j)}$	is the maximum number of MIMO layers (3GPP 38.802)
$Q_m^{(j)}$	is the bits per modulation symbol; depends on modulation scheme (3GPP 38.804)
$f^{(j)}$	is scaling factor (3GPP 38.306), 1, 0.8, 0.75 or 0.4 signaled via higher layers
$R_{\max}$	is LDPC code maximum number is 948/1024=0.92578125
$N_{\mathrm{PRB}}^{\mathrm{BW}(j),\mu}$	is the value of carrier configuration (3GPP 38.211);
$OH^{(j)}$	is the overhead due to signaling information: DL 0.14 for frequency range 1 (FR1), 0.18 for frequency range 2 (FR2)
SA_{DL}	is part of the slots allocated for DL in TDD mode (3GPP 38.213), only TDD mode used

3.2.2 Methodology proposed by METAS

METAS has proposed an SSB based method based on the extrapolation by multiplexing factors including time, frequency and space domain from measured RSRP of SSS RE [24]. The measurement method is based on the determination of the radiated field produced by the SSS of the downlink of the PBCH whereby the identification of the SS/PBCH beam identity (SS/PBCH block index) is required. The SSS is part of the SS/PBCH blocks which are distributed over a bandwidth of 3.6 MHz up to 7.2 MHz (for carrier frequency up to 6 GHz) within the NR downlink signal.

In a given location, the measurement is performed as follows: for each NR cell i, all measur-able SS/PBCH blocks must be identified in terms of their cell number i and SS/PBCH block index j (obtained by demodulating the DM-RS signal). Each SS/PBCH block with index j cor-responds to a PBCH antenna beam. For each SS/PBCH block (identified by its index j), the electric field strength $E_{i,j}^{\mathrm{SSS(RE)}}$ per RE of the SSS is measured. The electric field strengths $E_{i,j}^{\mathrm{SSS(RE)}}$ of all SS/PBCH blocks within a half frame are then added quadrati-cally to build a new value. The spatial maximum $E_{i,\max}^{\mathrm{SSS(RE)}}$ of this value has to be found within the measurement volume.

For each NR-cell i of the base station, the measured value the electric field strength has to be extrapolated to the reference operating mode (see Equation 10).

$$E_{i,h} = E_{i,\max}^{\mathrm{SSS(RE)}} \cdot K_i(\varphi_i, \theta_i) \quad (10)$$

with

$$E_{i,\max}^{\mathrm{SSS(RE)}} = \max\left(\sqrt{\sum_j \left(E_{i,j}^{\mathrm{SSS(RE)}} \right)^2} \right) \quad (11)$$

$$K_i(\varphi_i, \theta_i) = K_i^{\mathrm{SSS(RE)}} \cdot K_i^{\mathrm{Antenna}}(\varphi_i, \theta_i) \cdot K_i^{\mathrm{Stat}} \cdot K^{\mathrm{Duplex}} \quad (12)$$

where

$E_{i,h}$	is the extrapolated value of the electric field strength for cell *i* (in V/m)

$E_{i,\max}^{\mathrm{SSS(RE)}}$	Spatial maximum within the measurement volume of the quadratic sum of the SSS electric field strength per RE of all SS/PBCH blocks of cell *i*. The sum is performed on all available SS/PBCH blocks indexes j located within the same half frame
$E_{i,j}^{\mathrm{SSS(RE)}}$	Electric field strength (in V/m) per RE of the SSS of cell *i* and SS/PBCH block index *j*. This value is the quadratic mean of all measured SSS REs within the same SS/PBCH block
$K_i(\varphi_i, \theta_i)$	Global extrapolation factor for cell *i*. The global factor depends on the azimuth φ_i and on the elevation θ_i
$K_i^{\mathrm{SSS(RE)}}$	SSS extrapolation factor for cell *i*
$K_i^{\mathrm{Antenna}}(\varphi_i, \theta_i)$	Antenna Correction factor taking into account the different between the antenna diagram of the SS/PBCH signal of cell *i* and the antenna diagram of the total signal in the maximum permitted operation condition. The antenna correction factor depends on azimuth φ_i and on the elevation θ_i
φ_i	Azimuth, defined as the horizontal angle in a spherical coordinate system, of the measurement location with respect ot the transmit antenna of cell *i*
θ_i	Elevation, defined as the vertical angle in a spherical coordinate system, of the measurement location with respect ot the transmit antenna of cell *i*
K_i^{Stat}	Beam statistic factor for cell *i*
K^{Duplex}	Duplex factor

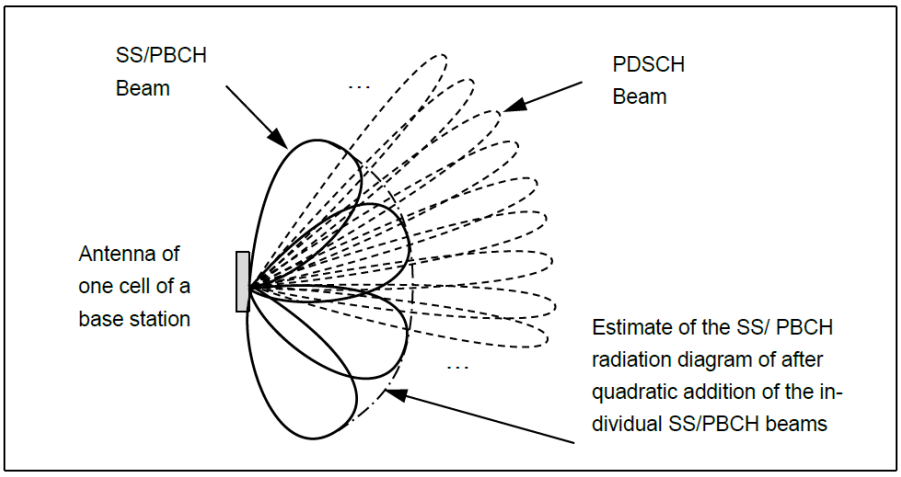

Figure 6 *Schematic representation of the horizontal radiation pattern of a NR-base station cell. The PDSCH beams are not all represented.*

For each cell i of the base station, the extrapolation factor for the SSS, $K_i^{\mathrm{SSS(RE)}}$ is defined as

$$K_i^{\mathrm{SSS(RE)}} = \sqrt{\frac{P_{i,\mathrm{Permitted}}}{P_i^{\mathrm{SSS(RE)}}}} \tag{13}$$

with

$$P_i^{\mathrm{SSS(RE)}} = \max_{\varphi_i, \theta_i} P_i^{\mathrm{SSS(RE)}}(\varphi_i, \theta_i) \tag{14}$$

$$P_i^{\mathrm{SSS(RE)}}(\varphi_i,\theta_i) = \sum_j P_{i,j}^{\mathrm{SSS(RE)}}(\varphi_i,\theta_i) \quad (15)$$

where

$P_i^{\mathrm{SSS(RE)}}$ Actual effective radiated power (ERP) per RE of the SSS of the SS/PBCH block of cell i in W. It corresponds to the maximum in all directions of the "summed SSS ERP radiation pattern"

$P_i^{\mathrm{SSS(RE)}}(\varphi_i,\theta_i)$ Summed SSS ERP radiation pattern obtained by summing the ERP radiated power per RE of all SS/PBCH beams as defined by the following equation

$P_{i,j}^{\mathrm{SSS(RE)}}(\varphi_i,\theta_i)$ Actual effective radiated power per RE in W of the SSS of the SS/PBCH block of cell *i* and index *j* in the direction given by the azimuth φ_i and by the elevation θ_i

$P_{i,\mathrm{Permitted}}$ Maximum permitted power ERP in W, take into account the signal of all antenna ports of cell *i*. i.e. PBCH, PDSCH, PDCCH

Note:

1. The maximum ERP $P_{i,\mathrm{Permitted}}$ refers to the maximum permitted ERP without any reduction.
2. The permitted power $P_{i,\mathrm{Permitted}}$ (according to the location datasheet) and the actual power of the reference signals $P_i^{\mathrm{SSS(RE)}}$ are provided by the network operator.
3. The actual power of the reference signals $P_i^{\mathrm{SSS(RE)}}$ is defined as the power per RE, and not as the total power of the SS/PBCH block.

For each cell i, the corresponding extrapolation antenna correction factor at azimuth angle φ_i and elevation angle θ_i, $K_i^{\mathrm{Antenna}}(\varphi_i,\theta_i)$ are defined as:

$$K_i^{\mathrm{Antenna}}(\varphi_i,\theta_i) = \begin{cases} 1 & if\ A_i^{\mathrm{SSS(RE)}}(\varphi_i,\theta_i) < 10 \text{ and } A_i^{\mathrm{SSS(RE)}}(\varphi_i,\theta_i) \le A_i^{\mathrm{Total}}(\varphi_i,\theta_i) \\ \frac{A_i^{\mathrm{SSS(RE)}}(\varphi_i,\theta_i)}{A_i^{\mathrm{Total}}(\varphi_i,\theta_i)} & if\ A_i^{\mathrm{SSS(RE)}}(\varphi_i,\theta_i) < 10 \text{ and } A_i^{\mathrm{SSS(RE)}}(\varphi_i,\theta_i) > A_i^{\mathrm{Total}}(\varphi_i,\theta_i) \\ K_{i,\max}^{\mathrm{Antenna}} & if\ A_i^{\mathrm{SSS(RE)}}(\varphi_i,\theta_i) \ge 10 \end{cases} \quad (16)$$

with

$$A_i^{\mathrm{SSS(RE)}}(\varphi_i,\theta_i) = \sqrt{\frac{P_i^{\mathrm{SSS(RE)}}}{P_i^{\mathrm{SSS(RE)}}(\varphi_i,\theta_i)}} \quad (17)$$

$$K_{i,\max}^{\mathrm{Antenna}} = \max_{\left\{\varphi_i,\theta_i \middle| A_i^{\mathrm{SSS(RE)}}(\varphi_i,\theta_i) < 10\right\}} A_i^{\mathrm{SSS(RE)}}(\varphi_i,\theta_i) / A_i^{\mathrm{Total}}(\varphi_i,\theta_i) \quad (18)$$

where the variables are defined as

$K_i^{\mathrm{Antenna}}(\varphi_i,\theta_i)$ Antenna correction factor taking into account the difference between the antenna diagram of the SS/PBCH signal of cell *i* and the antenna diagram of

the total signal in the maximum permitted operating condition. The antenna correction factor depends on the azimuth φ_i and on the elevation θ_i

$K_{i,\max}^{\text{Antenna}}$ Maximum value of the ratio $A_i^{\text{SSS(RE)}}(\varphi_i,\theta_i)/A_i^{\text{Total}}(\varphi_i,\theta_i)$, where the maximum is taken on all directions for which the attenuation $A_i^{\text{SSS(RE)}}(\varphi_i,\theta_i)$ of the SS/PBCH beam is less than 10 (corresponds to 20 dB).

$A_i^{\text{SSS(RE)}}(\varphi_i,\theta_i)$ Attenuation, of the summed SSS ERP radiation pattern of cell *i* in the direction given by the azimuth φ_i and by the elevation θ_i. The ratio is greater than 1, and it can sometimes be expressed in dB as $20\cdot\log_{10}(A_i^{\text{SSS(RE)}}(\varphi_i,\theta_i))$

$A_i^{\text{Total}}(\varphi_i,\theta_i)$ Attenation of the total signal radiation pattern of cell i in the direction given by the azimuth φ_i and by the elevation θ_i. The total radiatioin pattern corresponds to the envelope of all worst case radiation patterns in the permitted operation mode. This attenuation is defined as a voltage ratio in contrast to a power ratio greater than 1, and it can sometimes be expressed in dB as $20\log_{10}(A_i^{\text{Total}}(\varphi_i,\theta_i))$

While the definition of the beam statistical factor K_i^{Stat} is still under study, the conservative value of $K_i^{\text{Stat}}=1$ is currently being considered. The duplex factor $K^{\text{Duplex}}$is defined as:

$$K^{\text{Duplex}}=\begin{cases}\sqrt{r_{DL}} & \text{for TDD}\\ 1 & \text{for TDD with unknown } r_{\text{DL}}\\ 1 & \text{for FDD}\end{cases} \tag{19}$$

where r_{DL} denotes the maximum ratio of the downlink transmission time in a time interval. This choice is determined by the interpretation of the E-field limits as a quadratic time average of the E-field strength. Following the above, all NR cell-specific extrapolated electric field strength values could then be summed together as:

$$E_h=\sqrt{\sum_{i=1}^{n}E_{i,h}^2} \tag{20}$$

where

E_h Extrapolated electric field strength of NR for a given network, in V/m.

n Number of cells of the base station respectively of the installation.

Finally, the appreciation value, E_B could be obtained by summing the contributions $E_{\text{Network}_k,h}$ of all networks belonging to the same installation:

$$E_B=\sqrt{E_{\text{Network}_1,h}^2+E_{\text{Network}_2,h}^2+\cdots+E_{\text{Network}_n,h}^2} \tag{21}$$

4 Calibration methods and setup

The section shows the calibration methods and setup employed in this project. Prior to the start of the traceable measurement campaigns, the 128-element antenna array of the mMIMO BS, 4-element mMIMO testbed receiving end (Rx) antennas, RF power for the modulated signals of the mMIMO testbed and RF-EMF measurement systems needs to be calibrated. The following sub-sections show

some details of the calibration methods and their setup.

4.1 mMIMO Tx system

For the mMIMO Transmitting end (Tx) system, the multi-antenna calibration was performed in situ (in the same place that the experiments took place) by relying on an over-the-air (OTA)-based multi-channel transmitter calibration method. Given the inherent uncertainty of phase and delay caused by multiple RF channels, multi-channel calibration is a crucial factor that affects beamforming performance for a typical mMIMO antenna array. The traditional multi-channel calibration uses cable-based calibration methods or self-calibration by using a dedicated feedback circuit. The cable-based calibration method tends to require a long calibration period whenever a single-port receiver or a complex and costly multi-port receiver set-up is used. This can cause a problem over nonsynchronisation calibration on the multi-channel measurements, which becomes more severe as the number of antenna elements increases. On the other hand, the self-calibration method, which relies on dedicated hardware circuit, increases the testbed design complexity and, in turn, this makes it harder for the testbed to achieve its required performance.

Contrary to the aforementioned methods, the OTA-based transmitter multichannel calibration method does not require extra hardware circuits to obtain the RF calibration factors of multiple channels simultaneously. Thismethod achieves the best performance in an anechoic chamber, but it could still work effectively in a multi-path environment when verified by experimental measurements. More details about the RF multi-channel non-ideal factors of the mMIMO testbed, our multi-channel OTA calibration method, the verification of the calibration, and the beamforming performance after calibration within the real-world environment are provided in the following. The impairments (i.e. delay, amplitude, phase) due to the transmission through multiple RF chains for a typical mMIMO antenna array can be modelled as

$$x_{i,j}(t) = s\big(t - \tau_{i,j}\big)\alpha_{i,j}\exp\big(\mathrm{j}\phi_{i,j}\big), \tag{22}$$

where $x_{i,j}(t)$ is the actual waveform transmitted by the i-th row j-th column element of the array of the 128-element (configured as 16 × 8 array) antenna array when the RF channel delay, $\tau_{i,j}$, amplitude, $\alpha_{i,j}$, and phase, $\phi_{i,j}$, errors are accounted for, and $s(t)$ is the ideal transmit waveform without impairments. The signal $x_{i,j}(t)$ (or the part of it in the case of multipath channel) that travelled over the line-of-sight (LOS) path to the receiver can be expressed as

$$y_{i,j}^{\mathrm{LOS}}(t) = x_{i,j}(t)\beta_{i,j}\exp\big(\mathrm{j}\theta_{i,j}\big), \tag{23}$$

where $y_{i,j}^{\mathrm{LOS}}$ is the received signal corresponding to the LOS path of the transmit antenna element (i,j), $\beta_{i,j}$ is the amplitude of this LOS path, and $\theta_{i,j}$ is the phase of this LOS path.
A typical OTA-based calibration method uses a multi-antenna pilot scheme based on FDM that simultaneously transmit 10 antenna pilots for each orthogonal FDM (OFDM) symbol by inserting equally spaced comb pilots in the frequency domain. By using enough OFDM symbol resources, the scheme can realize the pilot pattern for very large numbers of active transmit antennas. At the receiver, the channel for each transmission antenna is estimated based on the pilot signal waveform.

According to the estimated frequency-domain channel response, the time domain channel impulse response (CIR) can be obtained. In an ideal environment such as a microwave anechoic chamber, estimations of the time delay, $\tau_{i,j}$, the combined amplitude, $\alpha_{i,j}\beta_{i,j}$, and the aggregated phase, $\phi_{i,j} + \theta_{i,j}$, of the direct LOS path can be easily obtained based on the CIR. Whereas in the multi-path scenario, it is necessary to consider the impacts of the parameter estimation accuracy such that a signal separation algorithm for multi-paths overlapped CIRs based on maximum likelihood (ML) criterion needs to be utilised to estimate these parameters. Once $\tau_{i,j}$ is estimated, it can then be easily

compensated for, i.e. its effect can be removed, in $x_{i,j}(t)$. The other important parameter that needs to compensated for to ensure that the array steers its beam in the desired direction is $\phi_{i,j}$.

In order to understand how $\phi_{i,j}$can be removed from $x_{i,j}(t)$, it is important to first understand how to extract $\phi_{i,j}$ from $\phi_{i,j} + \theta_{i,j}$. The phase of the LOS path for the the *i*-th row *j*-th column antenna element depends of the relative position between the transmit array and the receiver such that $\theta_{i,j}$ can be expressed as

$$\theta_{i,j} = \theta_{ref} + \Delta\boldsymbol{\theta}_{i,j}^{(a,b)}, \tag{24}$$

where θ_{ref} is the phase of the LOS path between one of the antenna elements, chosen as a reference element among all the antenna elements of the array, and the receiver. In addition, $\Delta\boldsymbol{\theta}_{i,j}^{(a,b)}$ is the *i*-th row *j*-th column component of the steering matrix $\Delta\boldsymbol{\theta}^{(a,b)}$that assumes the *a*-th row *b*-th column element of the array, i.e. antenna element (*a*, *b*), to be the reference element. The steering matrix $\Delta\boldsymbol{\theta}^{(a,b)}$ includes all the phase differences of any antenna element of the array relative to the phase of the reference element (*a*, *b*), such that

$$\Delta\boldsymbol{\theta}^{(a,b)} = \begin{bmatrix} (1-b)\Delta_1 + (1-a)\Delta_2 & \cdots & (16-b)\Delta_1 + (1-a)\Delta_2 \\ \vdots & \ddots & \vdots \\ (1-b)\Delta_1 + (8-a)\Delta_2 & \cdots & (16-b)\Delta_1 + (8-a)\Delta_2 \end{bmatrix}. \tag{25}$$

These phase differences account for the fact that each antenna element has a slightly different position relative to the receiver, with the position of element (a, b) as a reference position. In $\Delta\boldsymbol{\theta}^{(a,b)}$, Δ_1 and Δ_2 are the steering factors; they can be expressed, when considering that the distance between the elements are lambda/2 in both horizontal and vertical dimensions, as

$$\Delta_1 = \mathrm{j}\pi \sin(\varphi), \tag{26a}$$

$$\Delta_2 = \mathrm{j}\pi \sin(\vartheta), \tag{26b}$$

with φ and ϑ being the horizontal and vertical boresight angles of the transmission antenna array, respectively, and $\mathrm{j} = \sqrt{-1}$. For instance, if the antenna element (1, 7) is selected as a reference, as it shown in Figure 7, then

$$\Delta\boldsymbol{\theta}^{(1,7)} = \begin{bmatrix} -6\Delta_1 & \cdots & -\Delta_1 & 0 & \Delta_1 & \cdots & 9\Delta_1 \\ -6\Delta_1 + \Delta_2 & \cdots & -\Delta_1 + \Delta_2 & \Delta_2 & \Delta_1 + \Delta_2 & \cdots & 9\Delta_1 + \Delta_2 \\ \vdots & \ddots & \vdots & \vdots & \vdots & \ddots & \vdots \\ -6\Delta_1 + 7\Delta_2 & \cdots & -\Delta_1 + 7\Delta_2 & 7\Delta_2 & \Delta_1 + 7\Delta_2 & \cdots & 9\Delta_1 + 7\Delta_2 \end{bmatrix}, \tag{27}$$

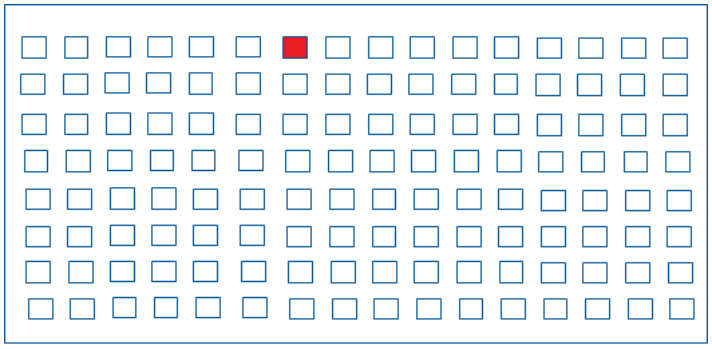

Figure 7 *Example of reference element for a 128-element antenna array; the antenna element (1, 7) is chosen as a reference for the OTA calibration procedure.*

By knowing $\Delta\boldsymbol{\theta}^{(a,b)}$, its effects can be removed for each antenna element from $\phi_{i,j} + \theta_{i,j}$ such that $\phi_{i,j} + \theta_{i,j} - \Delta\boldsymbol{\theta}_{i,j}^{(a,b)} = \phi_{i,j} + \theta_{ref}$. Then, by subtracting the residual phase of the *i*-th row *j*-th column antenna element, i.e. $\phi_{i,j} + \theta_{ref}$, from other element residual phases, it becomes possible to easily obtain the relative phase between all the elements of the array and to compensate for any phase misalignments. Thus, the effects of the of phase and delay caused by multiple RF channels can be removed from the transmission and beams can be steered in the desired direction. The different steps of the OTA-based calibration procedure are summarised in Figure 8.

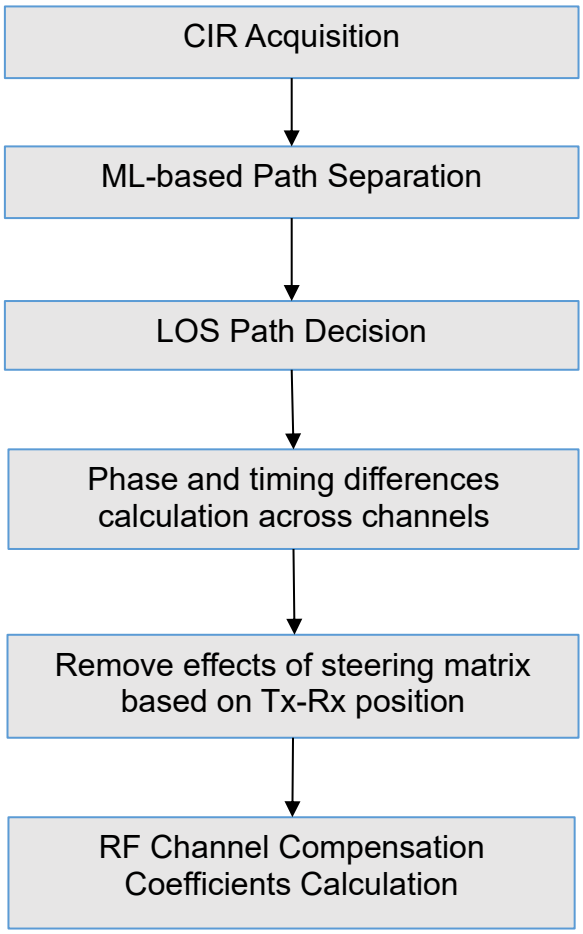

Figure 8 *Calibration OTA-based scheme: estimation and compensation procedure.*

The calibration of the mMIMO BS and its antenna array was performed in the same indoor and outdoor setup that used for the actual EMF experiments; more details about the measurement setup of the experiment are provided in D1 Sections 3 and 4. A receiver was placed 6 m away from the mMIMO BS, with the height of both equipment being similar. Several calibration tests were performed with each test producing independent time delay and phase estimations according to the procedure mentioned in Figure 8. The median of the estimated phase and delay in several tests was calculated based on the measurement results. Figure 9 shows the timing and phase difference across multiple channels before the calibration. From the results, it can clearly be seen that every four channels/antennas form a group in the sense that every channel/antenna within one of these groups has roughly the same timing. However, jitters can be seen between the different four-channel groups. This was somehow expected given the multiple subsystem's architecture of the mMIMO BS. Indeed, each MegaBEE transceiver module is composed of two sub-modules of four input/output RF ports, where each sub-module is internally synchronised with itself, while each sub-module is externally synchronised with the other modules via the White Rabbit time distribution system. Meanwhile, there

are significant phase differences between the channels regardless of whether they belong to the same sub-module. Figure 10 shows the timing and phase differences across multiple channels after the calibration. These results clearly demonstrate the effectiveness of the OTA-based calibration procedure. After applying it to the multiple RF channels, the phase and timing differences across most of them are adequately compensated, i.e. most of the delays are ten symbols long and most of the relative phase values are very close to 0 rad.

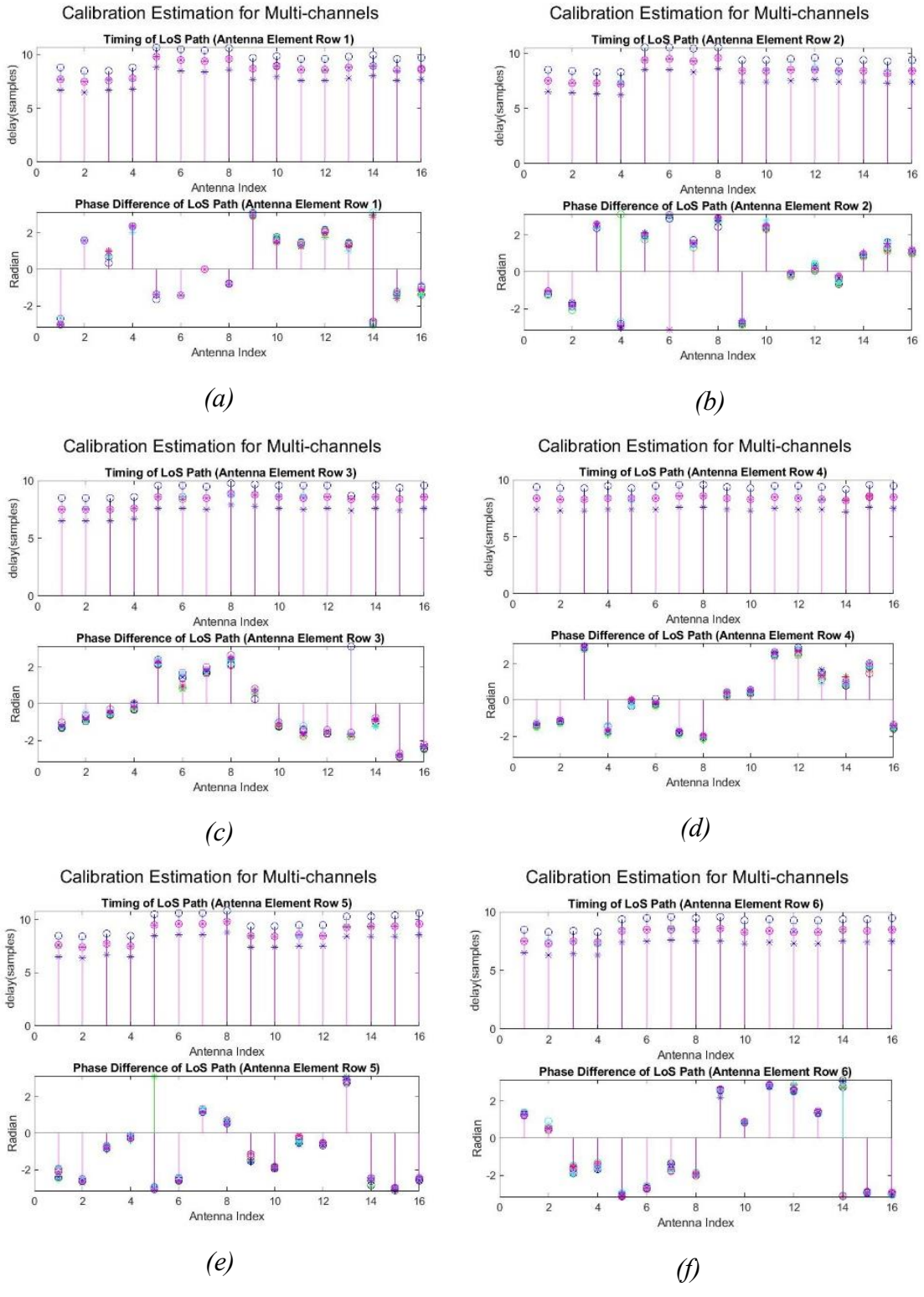

Figure 9 *Phase and timing differences across the multiple channels prior to OTA-based calibration for the first six row (i.e. (a) to (f)) of the 128-element mMIMO BS array.*

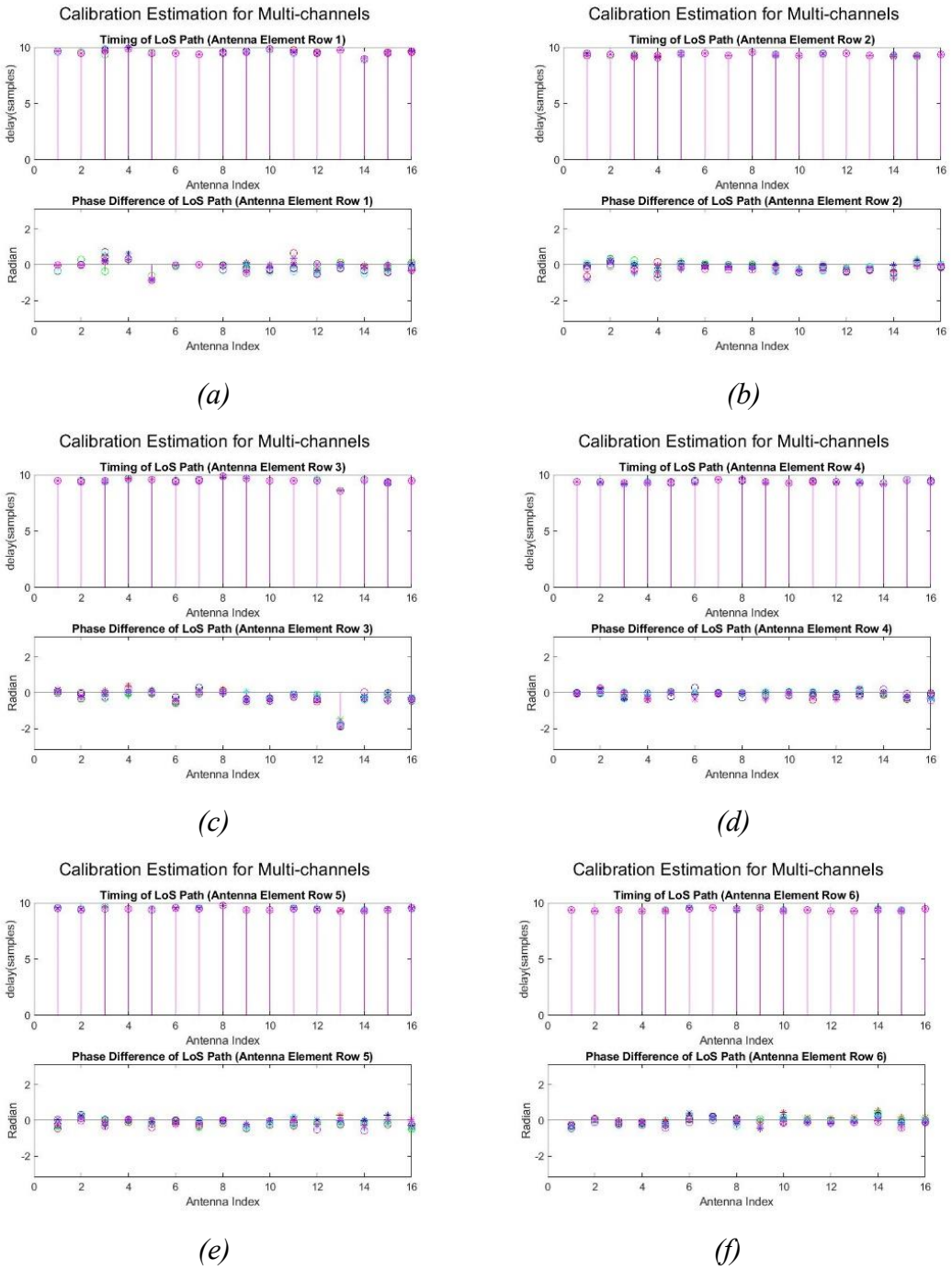

Figure 10 *Phase and timing differences across the multiple channels after OTA-based calibration for the first six row (i.e. (a) to (f)) of the 128-element mMIMO BS array.*

In order to validate the OTA-based calibration process, two beamforming tests were performed:

- In the first test, a beam was generated from the mMIMO BS at an angle of 9.46° from the boresight, i.e. pointing towards *the* point B, as it is depicted in Figure 11(a). At the same time, one receiver was moved over a 2-m distance, i.e. from point A to point C in Figure 11(a) (dark blue arrow), by steps of 25 cm. The results of the test in Figure 11(b) show that the received power gradually increases from point A to B, with the maximum reached at point B, and then

gradually decreases afterward from B to C. This is expected given that the beam points directly to B.

- In the second test, the receiver was placed at point B, while the beam was steered over 14° (following the orange arrow in in Figure 11(a)), i.e. from –1.46° to –15.46° of the boresight direction, by steps of 1°. Similar to first test, the results of the second test in Figure 11(c) show that the received power gradually increases when the beam is steered from –1.46° to –9.46° (i.e. the direction of point B – corresponds to 0° in Figure 11(c) since B is used as a reference point), with the maximum reached for a –9.46° angle, and then gradually decreases afterwards when the beam is steered from –9.46° to –15.46°, with a similar rate of increase/decrease on both sides of point B direction. This further validates the effectiveness of the OTA method for calibrating the mMIMO BS.

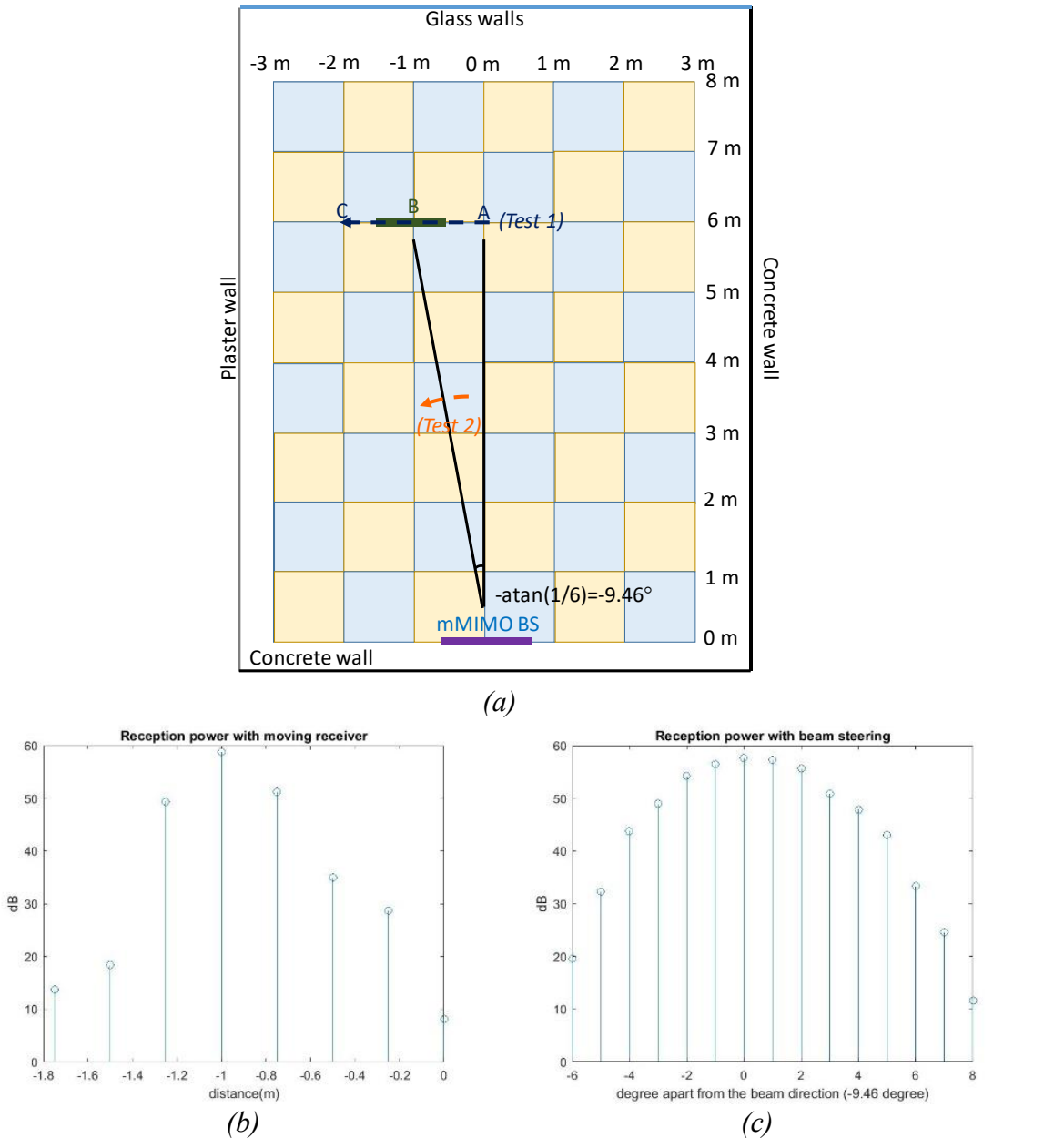

Figure 11 *Calibration test of the mMIMO BS via the OTA method: a) calibration test layout; b) first test results: moving receiver test; c) second test results: beam steering test.*

4.2 RF-EMF measurement systems

The RF-EMF measurements were made with two different receivers systems, namely, the Surrey RF-EMF measurement system and the Keysight RF-EMF measurement system. Both RF-EMF measurement systems were calibrated at the National Physical Laboratory (NPL).

4.2.1 Surrey RF-EMF measurement system

The Surrey RF-EMF measurement system consists of up to five sets of 4-dipole-element receive antenna array. This receiver system was calibrated component-wise with separate measurements made for the cables, MegaBEE receivers and antennas. The antennas were calibrated within the screened fully anechoic chamber facility at NPL [17] for both the antenna factor and the radiation pattern which was measured to estimate any uncertainty from the angle of arrival. The chamber has the following dimension of 7 m × 6.2 m × 6.2 m. The four-element Rx antenna arrays were calibrated by using the three antenna method in which the relevant losses are measured by using a Keysight PNA-X model N5242A vector network analyser (VNA). The MegaBEE receivers were calibrated for sensitivity to RF power received by using an NI-5681 power sensor.

4.2.1.1 Dipole antenna factor and cable loss

The antenna factor of an antenna relates the electric field the antenna is exposed to to the voltage produced at the antenna connector, therefore this parameter is essential to calculate the relationship between the electric field and the voltage that the MegaBEE receives. Measuremnet of the antenna factor was made on four of the Rx antenna elements which were selected as a sample for calibration at NPL. The antennas were calibrated whilst mounted on the metal mounting bar, taken from the trollys, using a substitution with a calibrated antenna of known performance. The relevant losses were measured by using a Keysight PNA-X model N5242A vector network analyser (VNA), which was also used to measure the loss of each of the four cables used to connect the antennas to the MegaBEE input. A photograph of the antenna factor measurement setup is shown in Figure 14.

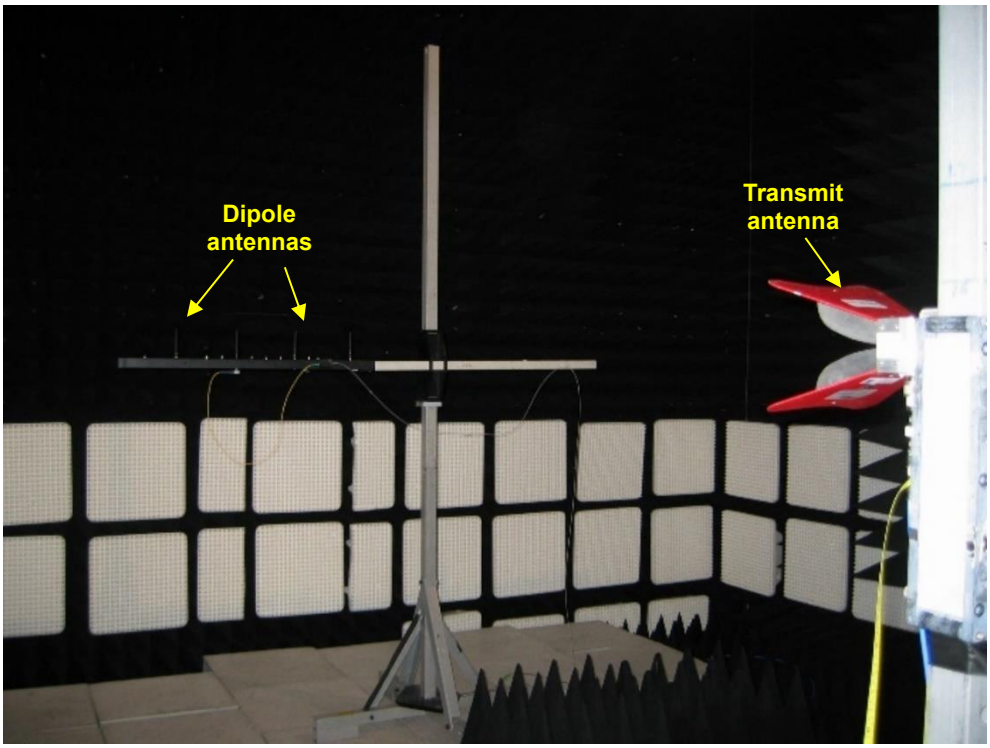

Figure 12 *Photograph of the dipole antennas during antenna factor measurement.*

A graph of the measured antenna factors is shown in Figure 13. Each of the 4 antennas was measured twice with the antenna reseated between measurements to simulate variations in performance cause by the flexible joint in the antenna. The average value from all measurement at the centre frequency of 2.63 GHz was measured as 37.5 dB/m.

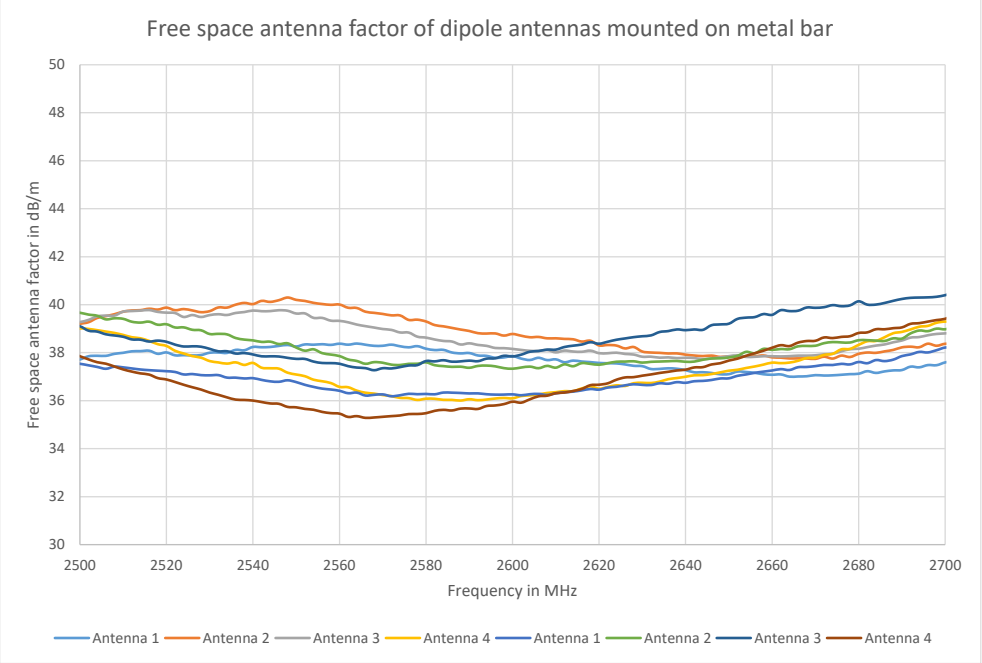

Figure 13 *Graph of measured dipole antenna factors*

4.2.1.2 Dipole radiation pattern

The radiation pattern of the four antennas was measured over a full rotation in azimuth axis and tests were also performed in elevation axis. The measurement setup is shown in Figure 14

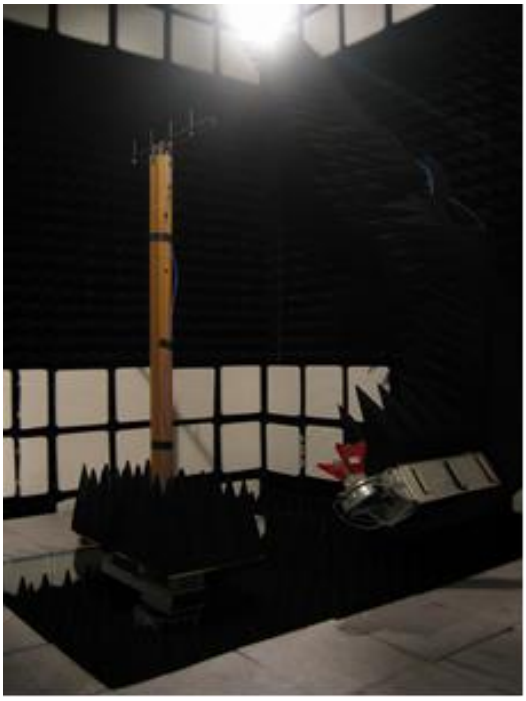

Figure 14 *Photograph of the dipole antennas during antenna radiation pattern measurement.*

The azimuth radiation pattern for the four antennas is presented in Figure 15. Measurements were made on each antenna at the centre frequency, and the upper and lower frequency range of mMIMO system, 2.61, 2.63, and 2.65 GHz respectively. The results show limited variation in the pattern around ±15° of the 0° boresight position, with the long edge of the bar facing the receiver, and then more vaiation, and higher received signal levels at greater angles. A possible explanation for this might be that there is constructive interference caused as the other antennas in the array begin to align as the bar rotates.

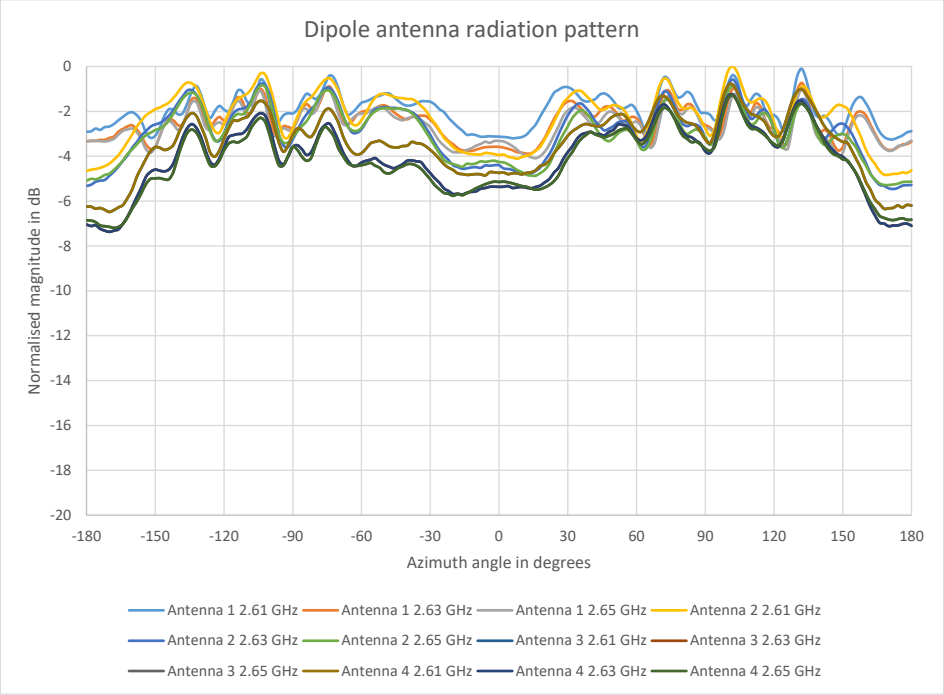

Figure 15 *Graph of measured dipole azimuth radiation patterns.*

4.2.1.3 MegaBEE reciever calibration

The MegaBEE receivers were calibrated for sensitivity to RF power by calibrating them against a NI-5681 power sensor. As depicted in Figure 16, a vector signal generator was used to generate a 5G waveform similar to those used in the main measurement campaign, this was passed through a directional coupler connected to both the power sensor and the MegaBEE, which was connected to the side arm as it was more sensitive. The coupling factor for the coupler was measured and this allowed a correction factor to be determined for the power measurement made by the MegaBEE. The vector signal generator (VSG) power level was adjusted allowing for correction factors to be determined at different frequencies.

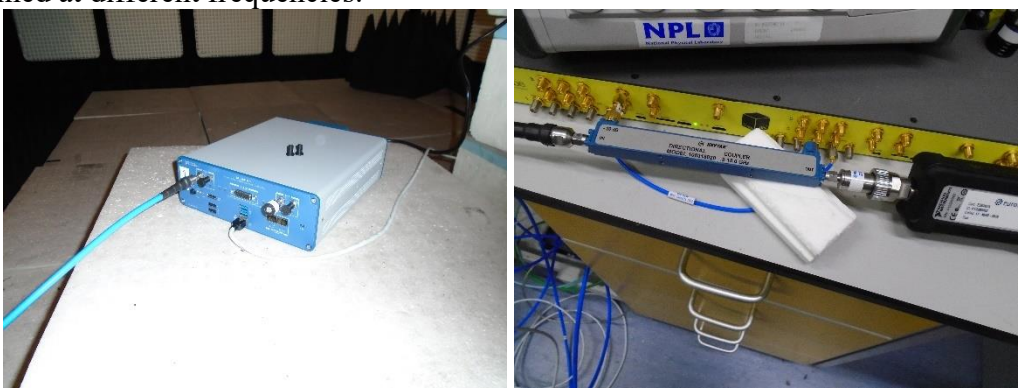

(a) *(b)*

Figure 16 *Photographs of the: (a) signal generator used to generate the calibration waveform; (b) directional coupler connected to the megabee and power sensor.*

4.2.2 Keysight RF-EMF measurement system

The Keysight RF-EMF measurement system, in which the channel power could be acquired, consists of a handheld Keysight FieldFox N9917B portable spectrum analyser (SA), and a an AGOS SDIA-6000 triaxial isotropic field probe. This system was calibrated at NPL in its Power Flux Density laboratory whereby the AGOS probe was placed against known electromagnetic plane wave generated by using established measurement techniques mentioned in Section 3.2.1, the measurement of which is depicted in Figure 17(a). The intensity of the field was adjusted and the measured value displaed on the FieldFox SA was used to calculate a calibration correction factor for the *x*-, *y*- and *z*-axis of the probe. Measurements were made at the centre frequency of 2.63 GHz and both ends of the instantaneous data bandwidth of 40 MHz of operation of the mMIMO system and at field levels of 0.1, 0.3, 0.5, 1.0, 3.0, 5.0 and 10 V/m which were chosen to cover the expected received levels.

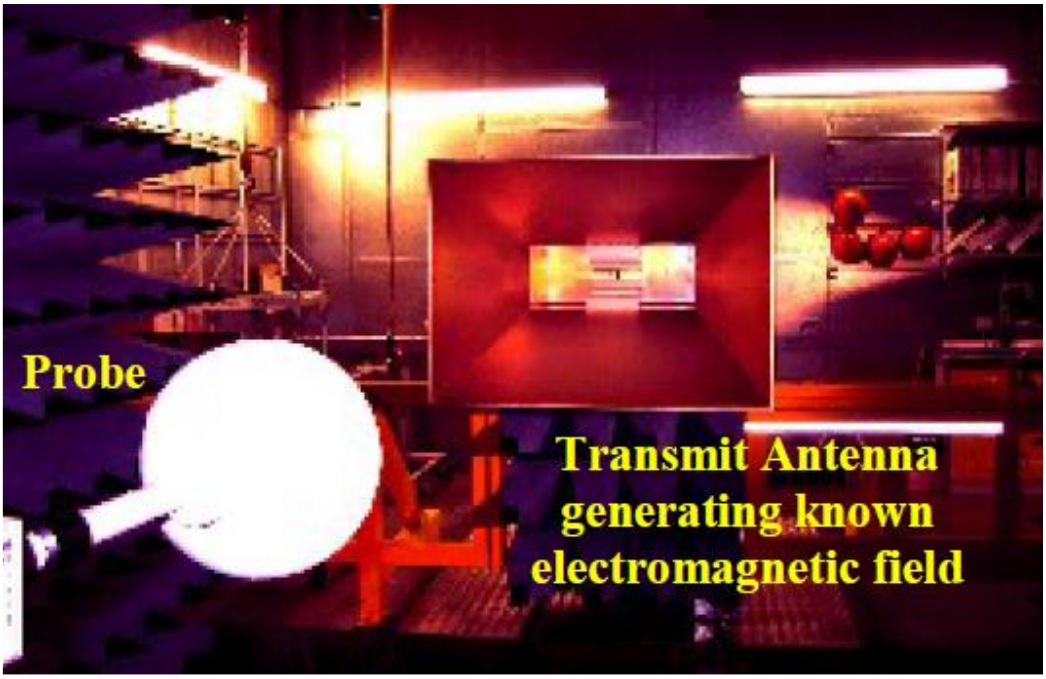

Figure 17 *Measurement setup for field probe calibration in NPL's power flux density laboratory.*

4.2.3 Verification of the RF-EMF reciver system calibrations

To verify that the calibration for the RF-EMF reciver systems was producing a consistent result comparison of electric field (E-field) measurements were carried out at NPL. The RF-EMF receiver systems were set up inside the screened fully anechoic chamber facility and the performance was compared while the systems were measuring the E-field generated by transmitting a modulated signal centred at a carrier frequency of 2.63 GHz with a 40 MHz instantaneous data bandwidth; and with a similar waveform to those used in the main measurement campaigns mentioned in the Deliverable report D1. A photograph of the measurements are shown in Figure 18.

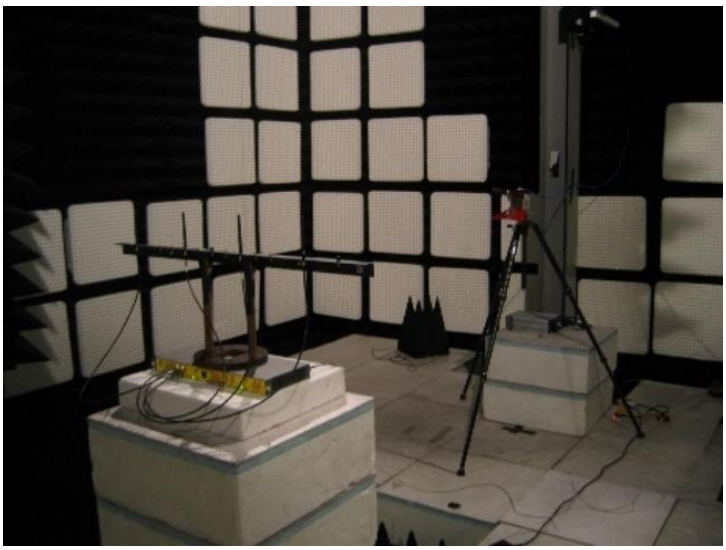

(a)

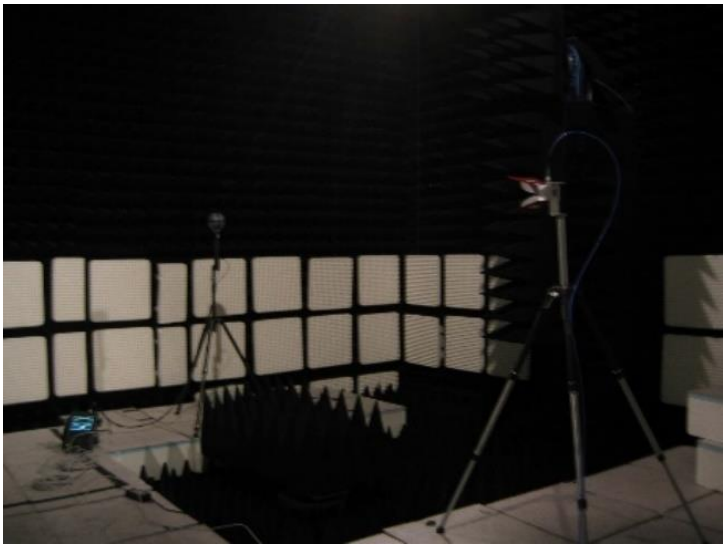

(b)

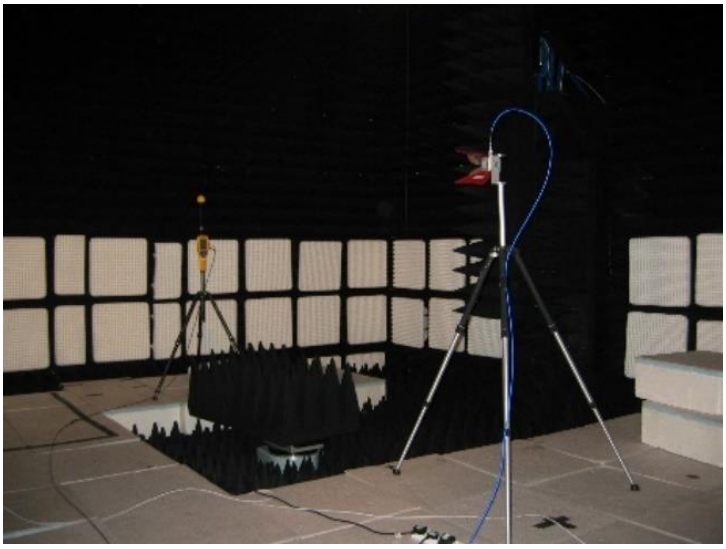

(c)

Figure 18 *Photographs of the electric field measurement systems showing (a) MegaBEE receiver with 4-dipole-element antenna array, (b) FieldFox system with AGOS field probe and (c) the Narda probe.*

A theoretical calculation and a calibrated commercial Narda probe were also used to further validate the obtained calibrated results. As depicted in Figure 19, the results of the various receive system and antenna elements match well with each other and they are more or less inline with the theoretically calculated results and probe results especially at low transmit power.

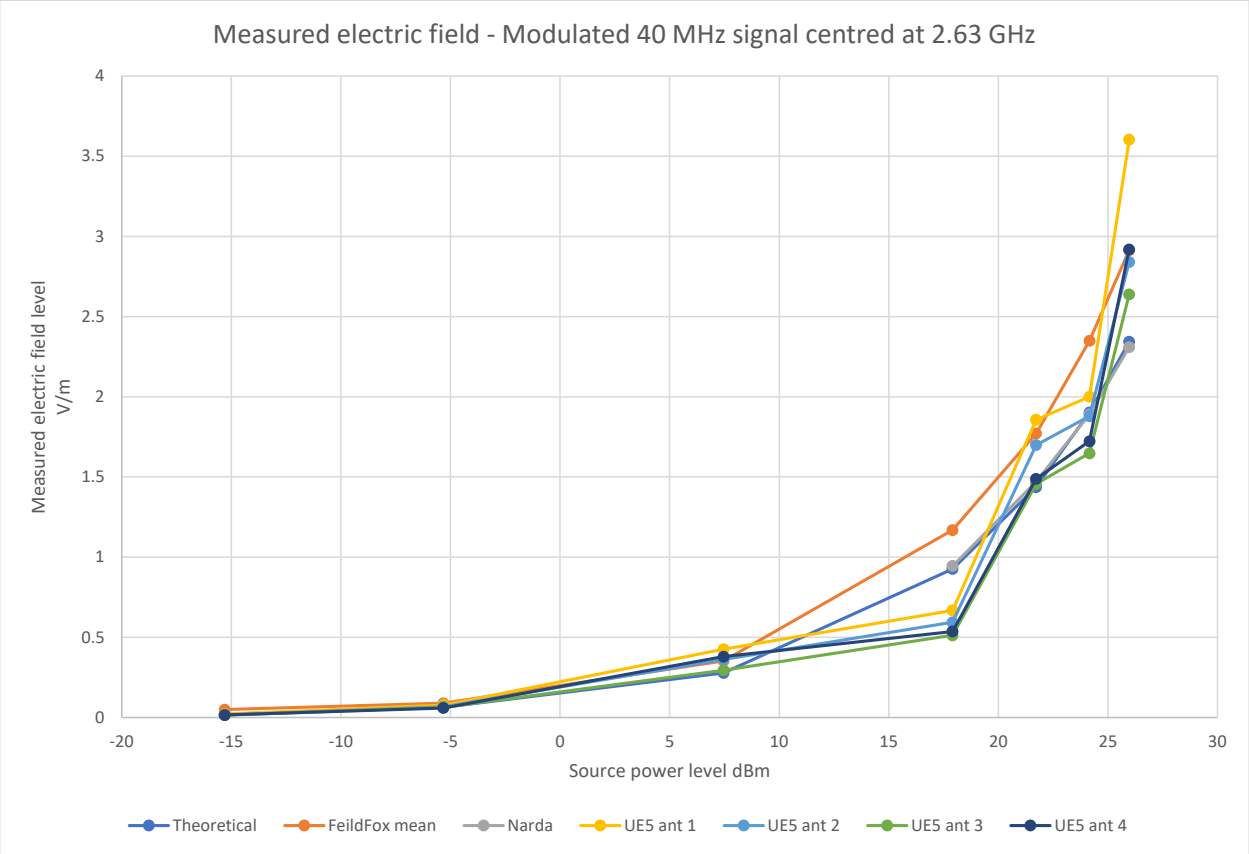

Figure 19 *Graph of theoretical and measured electric field.*

5 Hints and tips

This section provides a discussion on the hints and tips based on 'lesson learned' while carrying out the empirical measurements under A1.2.2 (indoor and outdoor / fixed beamforming) and A2.1.1 (outdoor / adaptive beamforming) (as shown in the Deliverable Report D1).

5.1 mMIMO system hardware impairment

While one envisages that the variations of the beam profiles and data rates are useful for assessing the spatial variation of RF-exposure surrounding the mMIMO testbed, to get insights into the effect on the stochastic nature of RF exposure generated by the non-ideal mMIMO beamforming operation due to potential hardware impairments and/or other factors (i.e. the phase coherency issue may have results in the beams not being well defined and that they may not steer in the expected direction) in the studied environment, thousands of E-field measurements were acquired without multi-channel OTA calibration carried out under the indoor measurement campaign with random active beams and payload data rate (the measurement setup is shown in Section 3.2 of Deliverable Report D1) where random pattern of transmission at the BS was implemented. An example comparison of the empirical cumulative distribution function (CDF) of these calibrated RF-EMF measurements of an

unnormalized mMIMO Tx system before and after the multi-channel OTA calibration is shown in Figure 20. From the comparison, we found that the as more beams are simultaneously activated the probability of higher value of RF-EMF is increased. Importantly, the difference between these results present an important observation for study over the stochastic nature of 5G NR mMIMO system while operating in non-ideal beamforming condition.

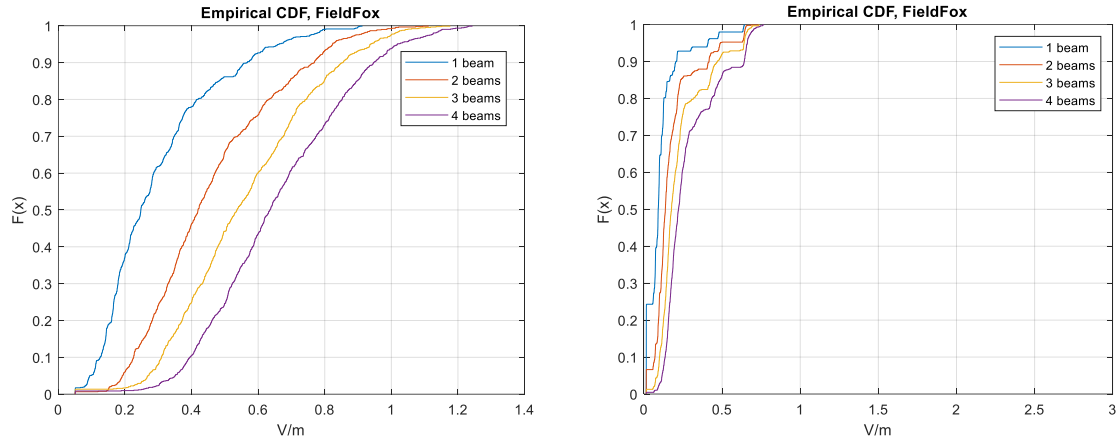

(a) *(b)*

Figure 20 *Empirical CDF of the calibrated RF-EMF acquired using the Keysight field probe with different number of simultaneous active beams from the mMIMO testbed in indoor environment: (a) without multi-channel OTA calibration; (b) with multi-channel OTA calibration (Figure 14 in D1).*

5.2 Black-box vs White-box approaches

The accurate implementation of statistical approaches/analyses to field strength based RF-EMF assessment method relies on the insight knowledge of 5G BS operation (such as number of UEs, their spatial distribution and traffic models). i.e. if all the 5G BS operation is known (i.e. 'white box approach'), one could gain useful insight knowledge into how these varying factors effect the 5G BS RF-EMF exposure levels at each UE. On the other hand, the accurate implementation of statistical approaches/analyses to SSB based RF-EMF assessment method relies on the correct demodulation and the use of suitable extrapolation technique to the measured 5G SSB RE signal under a specific 5G BS system configuration and traffic condition in the cell. i.e. no insight knowledge of 5G BS operation driven by UEs (i.e. 'black box approach') is required.

In this project, we have employed a user programmable mMIMO beamforming Tx system that is capable of generating fully compliant 5G NR waveforms for downlink communications for both indoor and outdoor measurement campaigns. This testbed (i.e. 'white box approach') is capable of mimicking the performance of a realistic 5G BS (i.e. 'black box approach'). The testbed provides flexible evaluation of various modulation schemes, new communication algorithms and protocols as well as enabling evaluation of the relevant OTA link performance. Operating with such system with specific knowledge on beam pattern profile(s) and data payloads, the project team is able to gain insight into the relevant statistics considering different number of users, user location and user data rate whereby such information would not be available for real 5G BS. i.e. there is no specific knowledge of beam pattern profile(s) for real 5G BS unless provided by the 5G BS manufacturers. This is due to the commercial sensitive nature over the implementation of 5G BS beamforming algorithm. Therefore, in practice, to carry out realistic 5G BS RF-EMF measurement one would need to stimulate data demand from UE terminal(s) using specific mobile applications (i.e. 'Apps') while positioning them at different practical test scearios, with all other 4G & 5G BSs turned off, where possible. While the "white box approach" is envisaged able to evaluate the precise 5G BS RF-EMF

assessment for a specific UEs' channel configuration, the "black box approach" is envisaged able to evaluate the overall 5G BS RF-EMF averaging across different UE configures under the same 5G BS cell data rate.

5.3 Implementation of statistical approaches

Using traditional method to design the compliance boundary (also known as exclusion zone) by using maximum transmit power in all directions would result in unrealistically large areas, making problematic for the operators to deploy mMIMO BSs with pre-existing 2G, 3G, and 4G BSs on sites [11]. Also, according to IEC 62232:2017 [8], the assessment of RF exposure is averaged over several minutes before comparing it to the allowed limits, and this is a very long period with respect to methods like beamforming update and UE scheduling, which happen at the BS every few milliseconds or even less. The principles of 5G exposure measurements based on the measurement of SSB signal have been presented in different contributions [20], [24]. Furthermore, in practice, one envisages that BSs are not always operated with 100% data payloads (i.e. they do not transmit at full power in each millisecond) and when multiple UEs are served by a BS, the power is split among different directions even with spatial multiplexing. Different contributions tend to demonstrate that the traditional approach for designing the compliance boundary might be over-conservative [11], [13], [14]. In particular, Reference [11] shows that using statistical approach for assessing the actual transmit power in more realistic scenarios by taking into account mMIMO BS operations (e.g. deployment scenarios and channel models), the compliance boundary turns out to be actually smaller when compared to the one computed with the conservative traditional method.

In this project, we have employed a user programmable mMIMO beamforming testbed system and traceable RF-EMF measurement system to provide extensive experimental-based evidence to understand the benefits of statistical approaches in assessing the stochastic nature of mMIMO. More specifically, the focus is given on consideration of various UE deployment scenarios and evaluate how the RF-EMF is varied in a practical system when realistic assumptions regarding number of active UEs, their spatial distribution and traffic models are taken into account. To understand the statistical variation of the RF-exposure (in V/m), the CDF of the RF-EMF exposure level from the mMIMO BS was derived against the interested factor, e.g. number of active UEs, etc. For example, Figure 21 show the empirical CDF of the calibrated RF-EMF acquired using the Keysight field probe with different number of simultaneous active beams from the mMIMO testbed in outdoor environment (Figure 22 in D1). Note that the power level of the mMIMO Tx system is not normalized (see Section 3.2.1 in D1 for details). As depicted in Figure 21, when looking at the 95th percentile of the CDF curve, the RF-EMF exposure level from the mMIMO BS is about 1.7 V/m and 2.4 V/m, for 1 active beam and 4 active beams, respectively. i.e. the exposure at a given point increases with the number of active UEs simultaneously by the non-normalised mMIMO BS. The implementation principles of statistical approaches are currently being investigated by international standardization bodies like the IEC to understand their benefits and limits for RF exposure assessment [8].

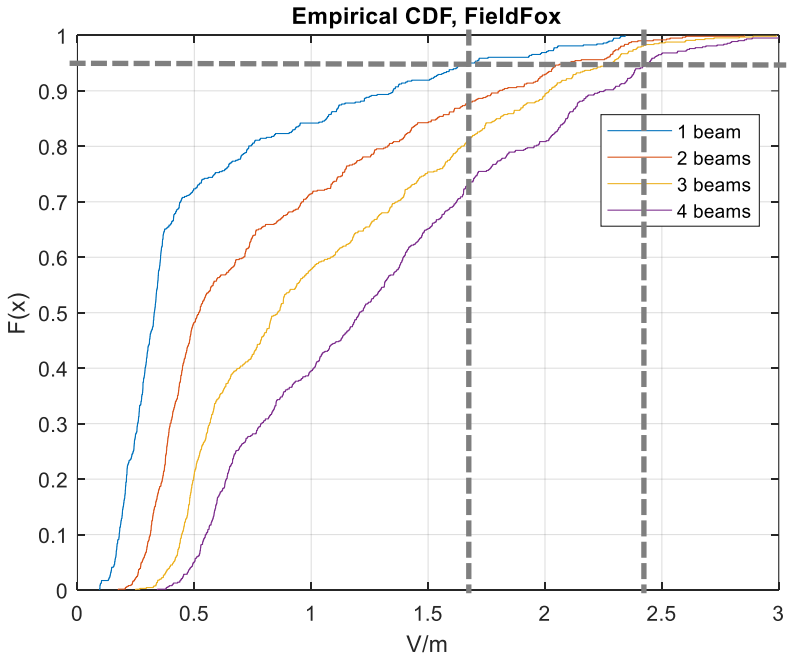

Figure 21 *The Empirical CDF of the calibrated RF-EMF acquired using the Keysight field probe with different number of simultaneous active beams from the mMIMO testbed in outdoor environment (Figure 22 in D1).*

5.4 Typical sources of uncertainty

The 5G NR technology is significantly more complex than previous generations. It implements a highly dynamic physical layer using a resource grid as well as stimulating multiple orientable beams using massive MIMO and adaptive MIMO antenna technologies in the downlink and uplink communications. The full NR resource grid contains signalisation channels that are constant in time, as well as traffic signals changing depending on the traffic demand. The following provides other sources of uncertainty that are typically envisaged over RF-EMF assessments.

5.4.1 Operating environment

While the measurement campaign is not being carried out in a controlled laboratory environment, the 'real-world' environmental effects are envisaged to contribute toward the RF-EMF measurement uncertainties. Several environmental factors for indoor and outdoor environments shall be practically considered while planning the measurement campaign. These including, for example, temperate, people movement and weather conditions, time of the day performing the measurements (hence interference sources and BS data resource variations), object in proximity (i.e. the selection of probe acquisition position), etc. A finding from evaluating the calibrated RF-EMF measurement results using the Surrey mMIMO testbed suggests that object in proximity (e.g. windor, wall, etc.) to the RF-EMF acquisition system could introduce strong non-LOS path.

5.4.2 Equipment setting and measurement setup

The full knowledge of the resource grid shall allow to provide much more information than any other broadband power-related measurements, and it does not require to put the transmit system in a test mode, or to interrupt the traffic. The effects of varying RF-EMF factors towards measurement uncertainty can't be neglected. In practice, the use of a field strength analyser attached to an isotropic field probe would enable practical evaluation of SSB based RF-EMF assessment at any location (see photos shown in Figure 22). Nevertheless, prior to any rigorous measurement campaign one would

have to ensure the correct equipment setting being applied at the acquisition system. For example, the targetted centre frequency of interest, the relevant data bandwidth, the detection mode (e.g. root-mean-square (RMS)-sum, *x*-, *y*- or *z*-axis field component), resolution bandwidth, etc. A photo of the channel power measurement setup for 5G NR using Keysight RF-EMF measurement system is shown in Figure 23. Also, it is important to note that for typical calibration of RF-EMF probe in PFD carried out using continues wave (CW), one may also introduce further measurement uncertainty over its use for acquisition of modulated RF-EMF signals.

(a) *(b)*

Figure 22 *Real-time monitoring of EMF for 5G NR using Keysight RF-EMF measurement system.*

Figure 23 *Channel Power measurement for 5G NR using Keysight RF-EMF measurement system.*

5.4.3 Measurement setup

In this project, while using the Surrey mMIMO testbed, the assumption is that all the fields have strong vertically polarized component (see a measurement setup photo in Figure 24). Nevertheless, probe polarization alignment may significantly affect the measurement accuracy when the probe is of single polarization as it may miss acquisition of field components in other polarization directions. On the other hand, the Keysight probe has three-axis in which their orientation is envisaged not critical for RMS-sum RF-EMF acquisitions.

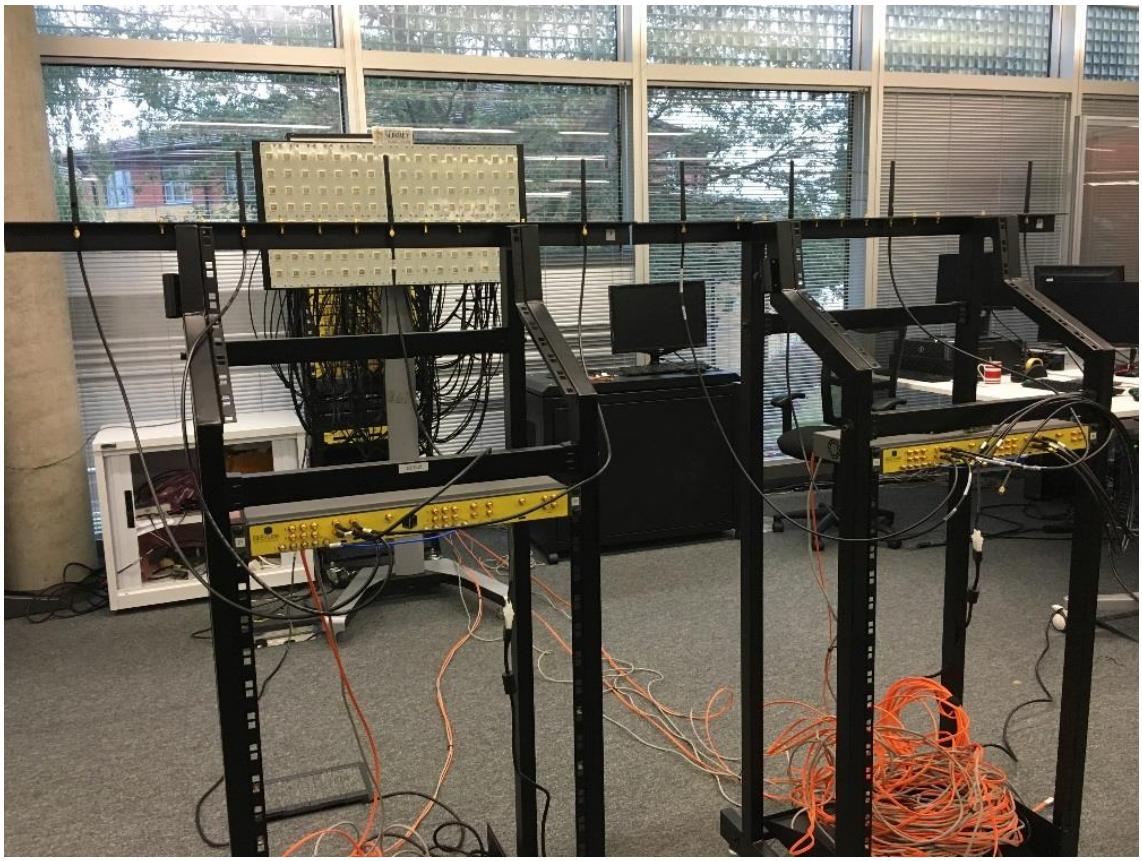

Figure 24 *A measurement setup for 5G NR RF-EMF evaluation using Surrey RF-EMF measurement system. Note that the dipole element is vertically polarized.*

5.4.4 Number of measurement samples

In this context, the inherent rule of statistics applies, i.e. the larger the number of measurement samples for evaluation the better the measurement accuracy. In this studies, the CDF could be used as a mean to assess whether the measurement samples have been sufficiently received.

6 Conclusion

This GPG has presented the guides for traceable RF-EMF measurement and data processing methods/protocols of mMIMO systems for 5G BS applications. The details of the relevant calibration procedures and setup for mMIMO beamforming and RF-EMF measurement systems have been provided. Also, the discussion on the hints and tips while carrying out the empirical measurements under A1.2.2 (indoor and outdoor / fixed beamforming) and A2.1.1 (outdoor / adaptive beamforming) (as shown in the Deliverable Report D1) have been discussed.

7 References

[1] L. Chiaraviglio, C. D. Paolo, G. Bianchi, and N. Blefari-Melazzi, "Is it safe living in the vicinity of cellular towers? Analysis of long-term human EMF exposure at population scale", *Proc. IEEE VTC-Spring*, Antwerp, Belgium, May 2020.

[2] M. A. Jamshed, F. He´liot, and T. W. C. Brown, "A survey on electromagnetic risk assessment and evaluation mechanism for future wireless communication systems", *IEEE J. Electrom. RF Microwave Med. Biol.*, 2020, 4(1), pp. 24–36.

[3] International Commission on Non-Ionizing Radiation Protection (ICNIRP), 'ICNIRP guidelines for limiting exposure to time-varying electric, magnetic and electromagnetic fields (up to 300 GHz)'. *Health Phys.*, 1998, 74(4), pp. 494–522.

[4] International Telecommunication Union (ITU), The impact of RF-EMF exposure limits stricter than the ICNIRP or IEEE guidelines on 4G and 5G mobile network deployment, 2018 [Online]. Available from: https://www.itu.int/rec/dologin_pub.asp?lang=e&id=T-REC-K.Sup14-201805-I!!PDF-E&type=items.

[5] L. Chiaraviglio, A.S. Cacciapuoti, G. Di Martino, et al. "Planning 5G networks under EMF constraints: state of the art and vision", *IEEE Access*, 2018, 6, pp. 51021–51037.

[6] Global System for Mobile Communication Association (GSMA), Arbitrary radio frequency exposure limits: impact on 4G network deployment, 2014 [online]. Available from: https://www.gsma.com/publicpolicy/wp-content/uploads/2014/03/Arbitrary-Radio-Frequencyexposure-limits_Impact-on-4Gnetworks-deployment_WEB.pdf.

[7] S. Blanch, J. Romeu, and A. Cardama, "Near field in the vicinity of wireless base-station antennas: an exposure compliance approach", *IEEE Trans. Antennas Propag.*, 2002, 50(5), pp. 685–692.

[8] International Electrotechnical Commission (IEC), IEC 62232:2017, "Determination of RF field strength, power density and SAR in the vicinity of radiocommunication base stations for the purpose of evaluating human exposure", IEC: Geneva, Switzerland, August 2017.

[9] B. Thors, A. Furuska¨r, D. Colombi, and C. To¨rnevik, "Time-averaged realistic maximum power levels for the assessment of radio frequency exposure for 5G radio base stations using massive MIMO", *IEEE Access*, 2017, 5, pp. 19711–19719.

[10] E. Degirmenci, B. Thors, and C. To¨rnevik, "Assessment of compliance with RF EMF exposure limits: approximate methods for radio base station products utilizing array antennas with beam-forming capabilities". *IEEE Trans. Electromagn. Compat.*, 2016, 58(4), pp. 1110–1117.

[11] P. Baracca, A. Weber, T. Wild, and C. Grangeat, "A statistical approach for RF exposure compliance boundary assessment in massive MIMO systems", *Proc. 22nd Int. ITG Workshop Smart Antennas (WSA)*, Bochum, Germany, March 2018, pp. 1–6.

[12] The Office of Communications (OfCom), Electromagnetic Field (EMF) measurements near 5G mobile phone base stations, technical report, April 2020 [online]. Available from: https://www.ofcom.org.uk/__data/assets/pdf_file/0015/190005/emf-test-summary.pdf.

[13] Agence Nationale des Fre´quences (ANFR), Assessment of the exposure of the general public to 5G electromagnetic waves, technical report, April 2020 [online]. Available from: https://www.anfr.fr/fileadmin/mediatheque/documents/5G/20200410-ANFR-rapport-mesures-pilotes-5G-EN.pdf.

[14] D. Colombi, P. Joshi, B. Xu, F. Ghasemifard, V. Narasaraju, C. To¨rnevik, "Analysis of the actual power and EMF exposure from base stations in a commercial 5G network", *Appl. Sci.*, 2020, 10(15), 5280.

[15] T. H. Loh, F. Heliot, D. Cheadle, and T. Fielder, “An assessment of the radio frequency electromagnetic field exposure from a massive MIMO 5G testbed”. *Proc. EuCAP 2020*, Copenhagen, Denmark, March 2020.

[16] T. H. Loh, D. Cheadle, F. Heliot, A. Sunday, and M. Dieudonne, “A study of experiment-based radio frequency electromagnetic field exposure evidence on stochastic nature of a massive MIMO system”. *Proc. EuCAP 2021*, Du¨sseldorf, Germany, March 2021.

[17] National Physical Laboratory, Small antenna radiated test range. 2020 [Online]. Available from: https://www.npl.co.uk/products-services/radiofrequency/smart-chamber.

[18] S. Persia, C. Carciofi, S. D'Elia, and R. Suman, “EMF evaluations for future networks based on massive MIMO”, *Proc. IEEE 29th Annu. Int. Symp. Pers. Indoor Mobile Radio Commun. (PIMRC 2018)*, Bologna, Italy, Sep. 2018, pp. 1197-1202.

[19] R. Pawlak, P. Krawiec, and J. Zurek, “On measuring electromagnetic fields in 5G technology”, *IEEE Access*, vol. 7, pp. 29826-29835, Mar. 2019.

[20] H. Keller, “On the assessment of human exposure to electromagnetic fields transmitted by 5G NR base stations”, *Health Phys.*, vol. 117, no. 5, pp. 541-545, Apr. 2019.

[21] International Electrotechnical Commission (IEC), IEC/TR 62669:2019. “Case Studies Supporting IEC 62232—Determination of RF Field Strength, Power Density and SAR in the Vicinity of Radiocommunication Base Stations for the Purpose of Evaluating Human Exposure”, IEC: Geneva, Switzerland, 2019.

[22] D. Franci, S. Coltellacci, E. Grillo, S. Pavoncello, T. Aureli, R. Cintoli, and M. D. Migliore, “An Experimental Investigation on the Impact of Duplexing and Beamforming Techniques in Field Measurements of 5G Signals”, *Electronics*, vol. 9, no. 2, p. 223, Jan. 2020.

[23] The 3rd Generation Partnership Project (3GPP) [Online]. Available: http://www.3gpp.org/.

[24] METAS, Technical Report: Measurement Method for 5G NR Base Stations up to 6 GHz, METAS-report 154.1-2020-5218-1016, February 2020 [Online]. Available: https://www.metas.ch/metas/en/home/dok/publikationen/meldungen/2020-02-18.html.

[25] A.-K. Lee, S.-B. Jeon and H.-D. Choi, “EMF Levels in 5G New Radio Environment in Seoul, Korea”, *IEEE Access*, vol. 9, pp. 19716-19722, 2021.

[26] S. Aerts *et al*., “In-situ Measurement Methodology for the Assessment of 5G NR Massive MIMO Base Station Exposure at Sub-6 GHz Frequencies”, *IEEE Access*, vol. 7, pp. 184658-184667, 2019.

[27] B. Selmaoui, P. Mazet, P. B. Petit, K. Kim, D. Choi, and R. de Seze, “Exposure of South Korean Population to 5G Mobile Phone Networks (3.4-3.8 GHz)”, *Bioelectromagnetics*, Vol. 42, No. 5, Jul. 2021, pp. 407 – 414.

[28] D. Choi and K. Kim, “The improvement study on the measurement method of the EMF human body exposure for 5G NR base station”, *the 2020 Joint Annual meeting of the Bioelectromagnetics Society and the European BioElectromagnetics Association (BioEM 2020)*, Oxford, UK, Jun. 2020.

[29] International Electrotechnical Commission (IEC), IEC 62232:2019, “Determination of RF field strength, power density and SAR in the vicinity of radiocommunication base stations for the purpose of evaluating human exposure”, IEC: Geneva, Switzerland, April 2019. Available: https://webstore.iec.ch/publication/62014.